1963

Random noise analysis in the Iowa State University UTR-10 reactor

Richard Arlen Danofsky
Iowa State University

RANDOM NOISE ANALYSIS IN THE IOWA STATE UNIVERSITY UTR-10 REACTOR

by

Richard Arlen Danofsky

A Dissertation Submitted to the
Graduate Faculty in Partial Fulfillment of
The Requirements for the Degree of
DOCTOR OF PHILOSOPHY

Major Subject: Nuclear Engineering

Approved:

Signature was redacted for privacy.

In Charge of Major Work

Signature was redacted for privacy.

Head of Major Department

Signature was redacted for privacy.

Dean of Graduate College

Iowa State University
Of Science and Technology
Ames, Iowa

1963

TABLE OF CONTENTS

I. SUMMARY

The purpose of this investigation was to study the crosscorrelation and cross power spectral density functions between the neutron density fluctuations in the two fuel regions of the Iowa State University UTR-10 reactor (commercial version of the Argonne National Laboratory Argonaut reactor).

A theoretical expression for the cross power spectral density function was derived. For high frequencies, ω greater than one radian per second, the derived relationship is of the form

$$\Lambda_{13}(\omega) = \frac{k^1}{(\omega^2 + \omega_1^2)(\omega^2 + \omega_2^2)} \quad , \tag{1}$$

where:

$\Lambda_{13}(\omega)$ is the cross power spectral density function;

ω is angular frequency;

k^1 is a constant

$\omega_1 = \frac{\beta}{\ell_o}$;

$\omega_2 = 2\frac{\epsilon_o}{\ell_o} + \frac{\beta}{\ell_o}$;

β is the total delayed neutron fraction;

ℓ_o is the prompt neutron lifetime;

ϵ_o is the reactivity coupling coefficient between the two fuel regions and accounts for the reactivity interaction between regions.

The cross power spectral function was measured and compared with the theoretical expression. The best estimates of ω_1 and ω_2 were obtained from a least square fit of the experimental data to the theoretical

expression. It was found that frequency components in the cross power spectral function above approximately 3 cps are quite rapidly attenuated. Thus the frequency spectrum interval occupied by the cross power spectral density function is of finite width.

The crosscorrelation function between fuel regions was first measured and then Fourier transformed to obtain the power spectral function. The neutron fluctuations in the two fuel regions were measured by ion chambers, converted to voltage fluctuations and displayed on a dual beam oscilliscope, and recorded on 35 mm movie film. The two traces on the developed film were sampled simultaneously at time intervals of 1/120 of a second for a total sampling time of approximately 10 seconds. The correlation and power spectral functions were calculated by means of an IBM 7074.

The prompt neutron lifetime ℓ_o was determined to be 3.04×10^{-4} seconds and ϵ_o , the reactivity coupling coefficient between regions, was found to be 5.17×10^{-3}. Thus, since ϵ_o is small, the two fuel regions are quite loosely coupled, that is, K_{eff} for each fuel region is approximately one when the two-core system is critical.

II. INTRODUCTION

A. Reactor Kinetics Studies

There are several important reasons for studying the kinetic behavior of a nuclear reactor. Two of the more important are (1) to determine system stability and (2) to establish parameters that are needed to characterize the reactor system in theoretical studies. As examples, stability of circulating fuel reactors has been predicted from kinetics studies (24), also results from kinetics studies have been used to estimate the power level at which a boiling water reactor would become unstable (10, 11). Accurate values of reactor parameters are needed by control system engineers for theoretical control system studies. In many cases reactor dynamic investigations are one important way of obtaining this information.

There are several standard experimental techniques that are used for studying reactor kinetic behavior. The transient behavior of the reactor after a step or ramp addition of reactivity has been studied (17, 28). This technique yields information on the self-regulating capabilities of the reactor and the shut-down mechanisms but other information is limited. Also, it is not always possible or even desirable to perform this type of experiment on every reactor. An extreme example of this type of kinetics study is the Borax series in which the reactor was destroyed after a large step addition of reactivity (30). Analysis in the frequency domain or as it is more commonly called, the transfer function or frequency response method, is probably the most important technique for reactor kinetics studies. The frequency response function

of a reactor is usually obtained by measuring the magnitude and the phase shift of the reactor output, normally considered to be neutron density, as the reactivity of the system is varied in a sinusoidal manner.

This frequency response or transfer function technique is closely related to the noise analysis methods used in this thesis. For this reason some of the important properties of a transfer function are discussed in the following section. The section on transfer functions is followed by sections in which some of the fundamental concepts related to noise analysis methods are discussed.

B. The Transfer Function

The transfer function is formally defined as the ratio of the Laplace transform of the output to the Laplace transform of the input for a system with all initial conditions taken as zero. This is normally written as

$$KG(S) = \frac{O(S)}{I(S)} \qquad (2)$$

where K is a constant, G(S) is usually written as a ratio of polynomials of powers of the complex parameter S and O(S) and I(S) are the Laplace transforms of the system output and input. The transfer function, KG(S), is a characteristic of the system and is independent of the form of the input. Physically, KG(S) is the Laplace transform of the impulsive response or weighting function of the system. If the transfer function is known for a system the output for an arbitrary input can be determined from Equation 2.

For reactor kinetic studies based upon transfer function measurements, the response of the system to a sinusoidal input is studied and the frequency response form of Equation 2 is obtained. The theoretical

expression for the frequency response function is obtained from Equation 2 by replacing the complex parameter S with $j\omega$ where j is the square root of minus one and ω is the frequency of the input expressed in radians per second (22, p. 126). The resulting expression is a complex quantity and contains information on both the phase lag and magnitude of the output.

As an example of how the transfer function of an actual system is obtained consider the derivation of the transfer function of the R-C circuit of Figure 1. The input is considered to be the voltage e_I and the output is the voltage e_o. Application of Kirchoff's law which states that the algebraic sum of the voltage drops around the loop must be zero yields the equations

$$-e_I + Ri + \frac{1}{C}\int_o^t idt = 0 \quad , \tag{3}$$

$$e_o = \frac{1}{C}\int_o^t idt \quad . \tag{4}$$

The Laplace transforms of Equation 2 and 3 are

$$-E_I(S) + RI(S) + \frac{1}{CS} I(S) = 0 \tag{5}$$

$$E_o(S) = \frac{1}{CS} I(S) \quad , \tag{6}$$

where capital letters are used to indicate the Laplace transforms of the time varying variables. The transfer function is obtained from Equations 5 and 6 by eliminating I(S) and solving for the ratio of output to input;

$$KG(S) = \frac{1}{RCS + 1} \quad . \tag{7}$$

The frequency response transfer function is obtained from Equation 7 by replacing S with $j\omega$;

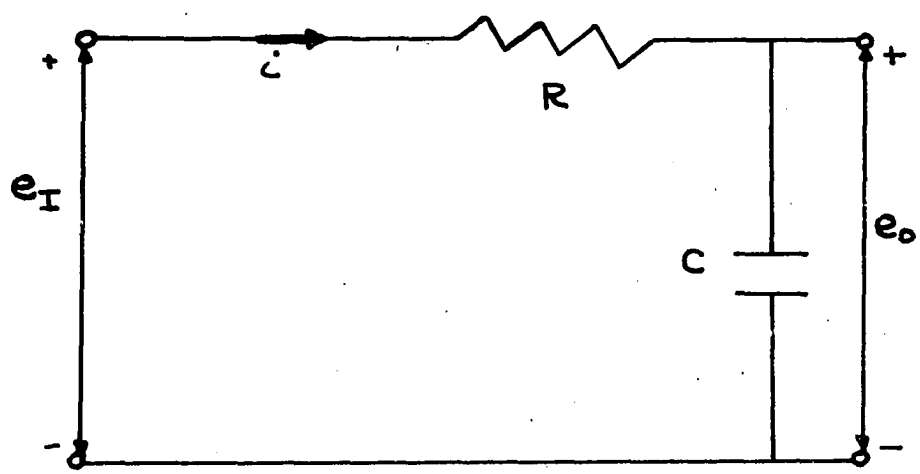

Figure 1. R-C circuit

$$KG(j\omega) = \frac{1}{RCj\omega + 1} \quad . \tag{8}$$

Equation 8 can also be expressed in terms of a magnitude and a phase angle;

$$KG(j\omega) = [(RC\omega)^2 + 1]^{-\frac{1}{2}} \angle - \tan^{-1} RC\omega \quad . \tag{9}$$

It is common practice to display transfer function information on Bode plots (22, p. 129) where magnitude and phase are plotted separately as functions of frequency. Magnitude, or as it is commonly called, the gain, is normally plotted in decibels, db, where the decibel is defined as 20 times $\log_{10}$ of the magnitude. On the Bode diagram magnitude in db and phase angle are plotted versus frequency on semilog paper with magnitude or phase angle on the linear scale and frequency on the log scale.

The example considered represents a very simple system and for most cases a more complicated expression for the transfer function or frequency response function results. The frequency response function for any system can be written in the general form

$$KG(j\omega) = K\frac{(1 + j\omega\ \tau_2)(1 + j\omega\tau_4)\ldots}{(j\omega)^n(1 + j\omega\tau_1)(1 + j\omega\tau_3)\ldots} \quad , \tag{10}$$

where τ_1, τ_2, τ_3, ... are parameters characteristic of the system and K and n are constants. The frequency equal to the reciprocal of the parameter τ is referred to as the break or corner frequency.

Frequency analysis methods can be used to determine the degree of stability of a system. For stability studies the phase shift at unity gain or zero db is determined. The phase margin which is defined as the amount the phase shift differs from 180 degrees is in turn approximately related to the damping of the system. Alternately, the appearance of resonance peaks in the gain portion of the transfer function can be used

as a qualitative indication of the onset of instability. The theoretical transfer function for a system can be determined from the differential equations describing the system and this can be used to obtain stability information or it may be necessary, as is often the case in practice, to resort to experimental studies to get accurate stability data since assumptions made in writing the differential equation of the system introduce unknowns into the theoretical expressions. For the experimental measurements the system is excited by a sinusoidal input and the magnitude and phase shift of the output is determined as the input frequency is varied.

A second useful application for experimental frequency response studies is the determination of system parameters. It can be observed from Equation 10 that the transfer function involves parameters τ_1, τ_2, τ_3, . . . which are characteristic of the system. These can be determined by curve fitting theoretical transfer function expressions to the experimental response data.

C. Open Loop Transfer Function for a Single Region Reactor

Some basic ideas related to nuclear reactor transfer functions are discussed in this section.

The transfer function of a system without feedback is referred to as the open-loop transfer function. For a reactor this corresponds to operation without the control system activated and at essentially zero power so that temperature and poison effects are negligible.

For the transfer function measurements of a reactor the system output is considered to be the neutron density and the input is the reactivity. One of the characteristics of the output of a reactor is

that it never assumes a negative value, as it could for example in an amplifier, hence it is not possible to treat the output as a sinusoidal function with zero average. When the reactivity of the reactor is varied in a sinusoidal manner the neutron density time variation is in the form of a small sinusoidal component superimposed on a steady state level. The customary procedure is to measure the change in magnitude and the phase shift of the sinusoidal component of the neutron density as the frequency of the input is varied.

The incremental reactor model is used to describe the system. For small variations of the neutron level about the steady state, the transfer function which relates the Laplace transform of the time varying component of neutron density $\Delta N(S)$ to the Laplace transform of the time dependent reactivity $\Delta K(S)$ can be derived. Schultz (23, p. 107) has shown that the open loop small signal or incremental transfer function is

$$\frac{\Delta N(S)}{\Delta K(S)} = \frac{n_o}{\ell} \frac{1}{S[1 + \sum_{i=1}^{6} \frac{\beta_i}{\ell(S + \lambda_i)}]} , \qquad (11)$$

where:

n_o = steady state neutron density

ℓ = prompt neutron lifetime

β_i = delayed neutron fraction of i^{th} group

λ_i = decay constant of i^{th} group of delayed neutrons.

One precaution must be observed in making reactor transfer function measurements. If the amplitude of the time dependent component of the neutron density becomes large enough to contribute significantly to the multiplication of the system the output will deviate from sinusoidal and the small signal or incremental reactor model will not be valid and

Equation 11 will not apply. This limits the magnitude of the reactivity input that can be used.

For purposes of discussion it is convenient to approximate Equation 11 with the transfer function for one group of delayed neutrons. For this case the transfer function can be written as

$$\frac{\Delta N(S)}{\Delta K(S)} = \frac{n_o \lambda}{\beta} \frac{(\frac{S}{\lambda} + 1)}{(\frac{S\ell}{\beta} + 1)} \quad . \tag{12}$$

The weighted average decay constant is λ and β is the total delayed neutron fraction. Since λ is generally small compared to $\frac{\beta}{\ell}$ it has been neglected in obtaining Equation 12. The block diagram for the open-loop incremental reactor model is shown in Figure 2. For a sinusoidal variation in reactivity S is replaced with $j\omega$ and the Bode diagram can be plotted as shown in Figure 3. The validity of the application of the transfer function approach to reactors was justified by experiments performed by Harrer et al. (13) on the CP-2 reactor at Argonne National Laboratory.

Several aspects of the reactor transfer function are of interest. It can be observed from Equation 12 that the constant portion of the transfer function is proportional to the steady-state neutron level. In servo-control terminology, the small signal sinusoidal gain of the reactor depends on the power level at which it is operated. This dependence of gain upon power level must be removed in the control loop before satisfactory automatic control can be achieved. Also, it can be observed from Figure 3 that the higher corner frequency occurs at $\frac{\beta}{\ell}$ radians per second in the one delayed neutron group approximation. The ratio of $\frac{\beta}{\ell}$ can be determined by fitting experimental frequency response data to

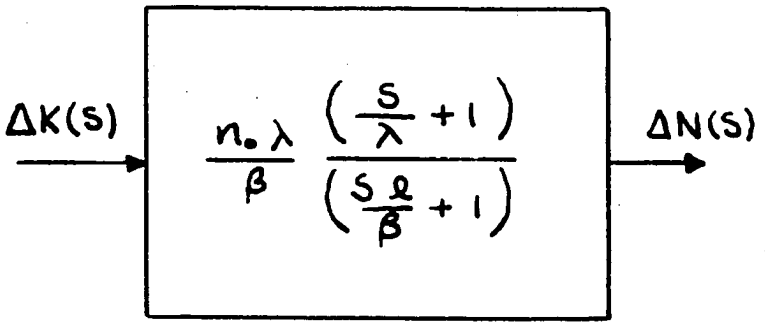

Figure 2. Open loop reactor block diagram

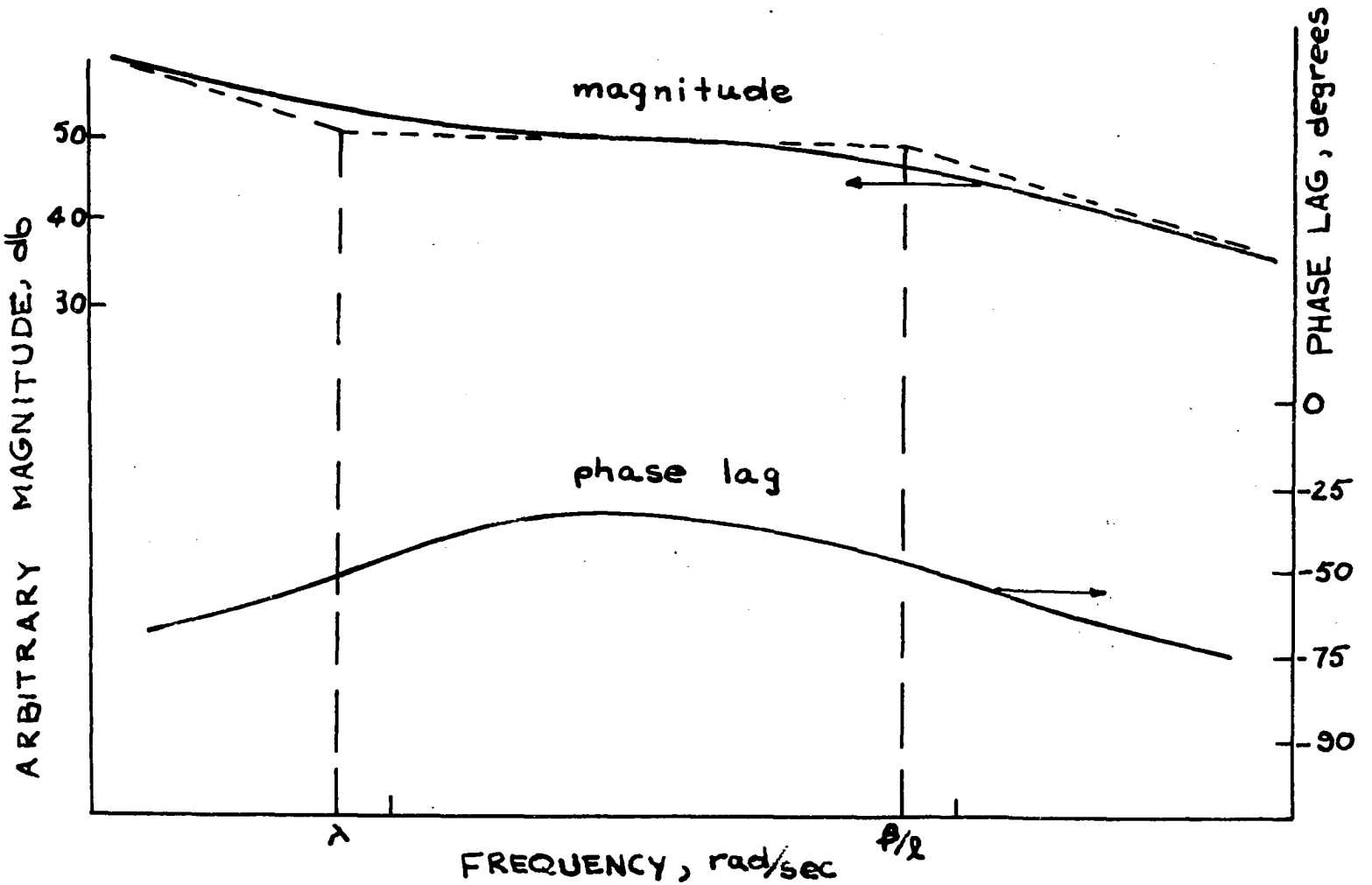

Figure 3. Bode diagram of open loop reactor frequency response function

theoretical transfer function curves. If β is known then neutron lifetime data can be obtained.

The effect of a control system, temperature coefficient, or poison buildup on the dynamic behavior of a reactor can also be accounted for from the transfer function approach. For these cases the closed loop transfer function is considered. A feedback loop for each effect to be considered is included on the reactor block diagram and an overall transfer function expression is written for the system. An example of this type of diagram is shown in Figure 4.

Several experimental techniques are available for obtaining frequency response data. One method is based upon output measurements obtained from the reactor when it is excited by sinusoidal reactivity input. A control rod or reactor oscillator is made to vary reactivity in a sinusoidal manner. The output of the reactor is measured with an ion chamber or other neutron detector and the magnitude and phase shift is determined as the input frequency is varied. This technique has become quite common in reactor work (7, 8). An alternate technique for obtaining transfer function data is one of a statistical approach. The processes taking place in a reactor are statistical in nature. It is possible to analyze the random variations in the output of the system and from these observations obtain transfer function data. Some of the concepts related to this type of analysis are discussed in the following sections. Advantages and limitations of various techniques are pointed out.

D. Autocorrelation and Power Spectral Density Relationships

Only linear systems will be considered in the following discussion

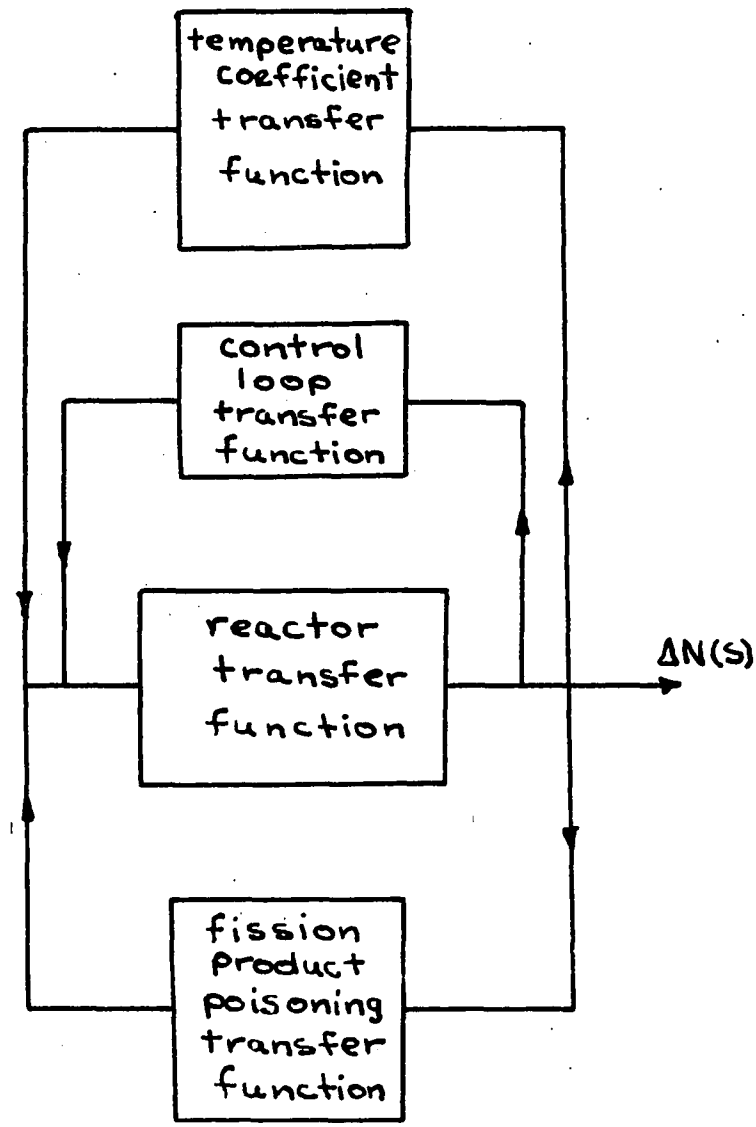

Figure 4. Multiple loop reactor block diagram

and it will be assumed that all random functions are ergodic, that is, their statistical properties do not change with time and ensemble averages over a large number of records may be replaced with a time average over a single record. For purposes of discussion a function is defined as random if its value at any time is predictable only in a statistical sense.

In the case of statistical analysis, measurements can be made either in the time domain in which case the autocorrelation function is used or in the frequency domain in which case the power spectral density is determined. It will be shown that the power spectral density is proportional to the square of the magnitude of the transfer function and therefore power spectral density measurements yield transfer function information.

The autocorrelation function of a random function x(t) is defined as

$$\zeta_x(\xi) = \lim_{T\to\infty} \frac{1}{T} \int_{-T/2}^{T/2} x(t)\, x\,(t + \xi)\, dt\,, \tag{13}$$

where ξ is a variable time displacement. The autocorrelation function is a measure of how well the function x(t) is correlated with itself after an elapsed time ξ. The maximum value of $\zeta_x(\xi)$ is $\zeta_x(0)$ and this is the mean square value of x(t). Also, $\zeta_x(\xi)$ is an even function of ξ.

It is shown by Bendat (4, p. 65) that the autocorrelation function and power spectral density function form a Fourier transform pair. That is, one can write

$$\zeta_x(\xi) = \frac{1}{2\pi} \int_{-\infty}^{\infty} \Lambda(\omega)\, e^{j\omega\xi}\, d\omega\,, \tag{14}$$

$$\Lambda\,(\omega) = \int_{-\infty}^{\infty} \zeta(\xi)\, e^{-j\omega\xi}\, d\xi\,, \tag{15}$$

where $\Lambda(\omega)$ is understood to be the power spectral density. From Equation 14 it can be seen that the mean square value of x(t) is

$$\overline{x^2(t)} = \zeta_x(0) = \frac{1}{2\pi}\int_{-\infty}^{\infty} \Lambda(\omega)\, d\omega \qquad (16)$$

which is proportional to the integral of the power spectral density over all frequencies. The inclusion of negative frequencies is merely a mathematical convenience and of course in the physical system only positive frequencies exist. If one thinks of x(t) as a voltage across a one ohm resistor then Equation 16 gives the energy dissipated in the resistor from all frequency components in x(t). Hence the name power spectral density for $\Lambda(\omega)$. There are basically two ways to obtain the power spectral density of a random function. The autocorrelation function can be calculated and then Fourier transformed or the power spectral density can be measured directly.

Consider a linear system which is described by a transfer function KG(S) and is excited by a random input with a power spectral density $\Lambda_f(\omega)$. The formal derivation of the relationship between input and output power spectral densities will now be outlined.

The system output, x(t), can be written in terms of the convolution integral as

$$x(t) = \int_0^{\infty} y(u)\, f\,(t - u)\, du \qquad (17)$$

where y(t) is the impulsive response of the system and is zero for negative time for a physically realizable system and f(t) is the input. The autocorrelation function of x(t) can be written as

$$\zeta_x(\xi) = \lim_{T\to\infty} \frac{1}{T}\int_{-T/2}^{T/2} \left[\int_0^{\infty} y(u)f(t-u)du \int_0^{\infty} y(y)f(t + \xi - v)\, dv\right]dt \qquad (18)$$

utilizing Equations 13 and 17. If integration with respect to t is performed first and the limiting process is moved inside the integral Equation 18 becomes

$$\zeta_x(\xi) = \int_0^\infty \int_0^\infty y(u)\ y(v)\ [\lim_{T\to\infty} \frac{1}{T} \int_{-T/2}^{T/2} f(t-u)f(t+\xi-v)dt]dudv. \qquad (19)$$

From the definition of the autocorrelation function;

$$\lim_{T\to\infty} \frac{1}{T} \int_{-T/2}^{T/2} f(t-u)f(t+\xi-v)dt = \zeta_f(u-v+\xi) \quad , \qquad (20)$$

the autocorrelation function of the **input**.. Thus Equation 19 can be written as

$$\zeta_x(\xi) = \int_0^\infty \int_0^\infty y(u)\ y(v)\ \zeta_f(u-v+\xi)\ dudv. \qquad (21)$$

Upon taking the Fourier transform of both sides of Equation 21 it follows that

$$\Lambda_x(\omega) = \int_{-\infty}^\infty [\int_0^\infty \int_0^\infty y(u)y(v)\ \zeta_f(u-v+\xi)dudv]\ e^{-j\omega\xi}d\xi \qquad (22)$$

where $\Lambda_x(\omega)$ is the power spectral density of the output. An interchange of the order of integration and the change of variable, $\kappa = u-v+\xi$, results in

$$\Lambda_x(\omega) = \int_0^\infty y(u)\ e^{j\omega u}du \int_0^\infty y(v)\ e^{-j\omega v}dv \int_{-\infty}^\infty \zeta_f(\kappa)e^{-j\omega\kappa}d\kappa. \qquad (23)$$

The first term is the complex conjugate of the frequency response function, the second is the frequency response function and the third is the power spectral density of the input. Equation 23 can be written as

$$\begin{aligned}\Lambda_x(\omega) &= KG(-j\omega)\ KG(j\omega)\ \Lambda_f(\omega) \\ &= |KG(j\omega)|^2\ \Lambda_f(\omega) \quad . \end{aligned} \qquad (24)$$

This is a very important relationship and is the basis for dynamic system

analysis using power spectral density measurements. It states that the square of the magnitude or modulus of the system transfer function is given by the ratio of the power spectral density of output to input. Thus if the input and output power spectral densities can be determined, the gain portion of the transfer function can be established.

There are several important disadvantages in using power spectral density measurements for the determination of system transfer functions; (1) no phase shift information is obtained, (2) other system noise can make accurate measurement difficult and (3) it is often quite difficult to ascertain the exact form of the system input.

These remarks are general and apply equally well to any physical system. In the case of a nuclear reactor system several advantages of the statistical approach become apparent. The processes taking place in a reactor are statistical in nature and result in a random driving function for the system. One of the problems associated with external reactivity oscillation is that care must be taken to insure that operation is in a range where the incremental reactor model is valid. This problem is circumvented in statistical analysis since the system output represents the minimum obtainable. A second important advantage is that the reactor system is not altered by the introduction of a mechanical oscillator or control rod as in the case of external oscillation studies.

Previous investigators have assumed that the reactor input noise spectrum is invariant with respect to frequency at least over the range of frequencies important in reactor kinetics measurements (band limited white noise). The power spectral density of this form of input is a constant and thus it can be seen from Equation 24 that a measurement of

the power spectral density of the output yields a quantity proportional to the square of the magnitude of the transfer function. This is the basis for a large amount of the work reported in the literature on power spectral density measurements in nuclear reactors.

E. Crosscorrelation and Cross Power Spectral Relationships

The crosscorrelation function between two random variables x(t) and f(t) is given by

$$\zeta_{fx}(\xi) = \lim_{T \to \infty} \frac{1}{T} \int_{-T/2}^{T/2} f(t)\, x(t + \xi)\, dt \,, \tag{25}$$

where ξ is again defined as a variable time displacement. The cross power spectral density function and crosscorrelation function also form a Fourier transform pair (4, p. 69). That is

$$\zeta_{fx}(\xi) = \frac{1}{2\pi} \int_{-\infty}^{\infty} \Lambda_{fx}(\omega)\, e^{j\omega\xi} d\omega \,, \tag{26}$$

$$\Lambda_{fx}(\omega) = \int_{-\infty}^{\infty} \zeta_{fx}(\xi)\, e^{-j\omega\xi} d\xi, \tag{27}$$

where $\Lambda_{fx}(\omega)$ is the cross power spectral density function between the two signals. Some significant properties of the crosscorrelation function are (1) the crosscorrelation function is not an even function, (2) a shift in x(t) yields the same result as a shift of the same amount of f(t) in the opposite direction, and (3) $\zeta_{fx}(\xi)$ does not necessarily possess a maximum at ξ equal to zero. The crosscorrelation function is a measure of the interdependence of two variables and is zero if they are independent or uncorrelated. For example the crosscorrelation function of two sinusoidal signals of different frequencies is identically zero.

It can be shown formally that measurement of the cross power spectral density function between the input to a linear system and output

combined with the input power spectral density function enables one to find the phase angle as well as the magnitude of the transfer function. The output of the system, x(t) can be written in terms of the impulsive response of the system, y(t), and the input, f(t), by means of the convolution integral of Equation 17. The crosscorrelation function can then be written as

$$\zeta_{fx}(\xi) = \lim_{t\to\infty} \frac{1}{T} \int_{-T/2}^{T/2} f(t) \left[\int_{o}^{\infty} y(u)\, f(t-u+\xi)\, du \right] dt. \qquad (28)$$

Upon interchanging the order of integration and utilizing the definition of the autocorrelation function of the input, $\zeta_f(\xi)$, Equation 28 can be written as

$$\zeta_{fx}(\xi) = \int_{o}^{\infty} y(u)\, \zeta_f(\xi-u)\, du \quad . \qquad (29)$$

The cross power spectral density function is then found by Fourier transforming Equation 29;

$$\Lambda_{fx}(\omega) = \int_{-\infty}^{\infty} e^{-j\omega\xi} \left[\int_{o}^{\infty} y(u)\, \zeta_f(\xi-u)du \right] d\xi \ , \qquad (30)$$

where $\Lambda_{fx}(\omega)$ is the cross power spectral density function. Upon interchanging the order of integration and substituting $\alpha = \xi - u$, Equation 30 can be written as

$$\Lambda_{fx}(\omega) = \int_{o}^{\infty} y(u)\, e^{-j\omega u} du \int_{-\infty}^{\infty} [\zeta_f(\alpha)\, e^{-j\omega\alpha}\, d\alpha]$$

$$= KG(j\omega)\, \Lambda_f(\omega) \quad . \qquad (31)$$

Thus, $KG(j\omega)$ is determined as the ratio of $\Lambda_{fx}(\omega)$ to $\Lambda_f(\omega)$. Since $\Lambda_f(\omega)$ is real $\Lambda_{fx}(\omega)$ is complex and contains both phase and magnitude information. Equation 31 is a very important relationship in cross-correlation work. The usual procedure is to measure the correlation

functions and then transform them to find the power spectral functions.

F. Purpose of Investigation

The purpose of this work is to apply crosscorrelation methods to a kinetic study of the Iowa State University UTR-10 reactor. The core of this reactor is in the form of two slabs of fuel elements separated by approximately 18 inches of graphite. A theoretical expression is derived for the cross power spectral density function between the neutron fluctuations in the two fuel regions when the reactor is critical. The resulting expression is a function of the neutron lifetime and the reactivity coupling between regions.

The crosscorrelation and cross power spectral function are measured and compared with the theoretical equation. The experimental data are used to establish the best estimate, in the least squares sense, of the neutron lifetime and the reactivity coupling between fuel regions for the reactor.

III. LITERATURE SURVEY

The purpose of this section is to discuss some of the more interesting and important applications of random-noise theory to the analysis of nuclear reactor systems. Early efforts in this area are discussed as well as current work. Both autocorrelation and crosscorrelation techniques are considered.

The application of noise-analysis methods to reactor kinetic studies is a relatively new technique although the mathematical relationships of noise analysis were known years earlier. Moore (18) was one of the first investigators to discuss the application of Equation 24 to nuclear reactor systems. This was followed by power spectral density measurements reported by Cohn (6). Griffin and Lundholm (12) compared the prompt neutron lifetime of the SRE and KEWB reactors as determined by power spectral density measurements and reactor oscillator techniques. Both methods resulted in approximately the same lifetime. They reported that the oscillation technique was found to be better suited for lifetime measurements in reactors where the prompt lifetime corner frequency is less than 5 cps and noise analysis is more suitable for reactors with corner frequencies above 20 cps.

Thie (26) measured the autocorrelation function of the EBWR. The power spectral density was then obtained by Fourier transforming the autocorrelation function. Information on the reactivity input noise spectrum was obtained by comparing transfer function data obtained from rod oscillator tests with the output noise spectrum. An indication of a change in reactor stability was obtained from a comparison of the height

of reasonance peak in the noise spectrum at 20 and 46 megawatts. As power was increased the resonance peaks became more pronounced thus indicating a decrease in stability with increase in power.

Thie (25) also discussed the use of power spectral density measurements to detect PU-239 build up. This is based on a measurement of changes in the prompt neutron lifetime corner frequency. It was indicated that the ratio of PU-239 to U-235 atoms can be determined to within 0.01. Thus an estimate of Plutonium buildup can be obtained from a comparison of power spectral density measurements at the beginning and at the end of the core life.

Batch and Ball (3) described the use of noise analysis to measure reactor stability on the nuclear ship Savannah. Power spectral measurements showed changes in resonnance peaks as operating conditions changed from dockside to heavy sea operation.

Kasten (15) has reported that changes in fuel stability in the HRE at Oak Ridge resulted in changes in the autocorrelation and power spectral density functions.

Uhrig (27) has used power spectral density measurements to determine the shutdown margin for a subcritical reactor. With this technique it would be possible to determine the effective multiplication factor for a lattice without disturbing the assembly. This offers advantages from the safety standpoint for reactor operation.

Balcomb et al. (1) have applied a crosscorrelation method to determine the closed loop impulsive response of the Kiwi-A3 reactor. A programmed white noise input was introduced as a reactivity demand into the reactor control system and the system input and output were crosscorrelated. It

can be shown that the crosscorrelation function is proportional to the impulsive response of the system for this type of input. The impulsive response was then Laplace transformed to obtain the system transfer function. Some of the advantages of the method are (1) measurements can be taken without interferring with normal operation of the system, (2) small input amplitude perturbations are used so it is not hazardous, and (3) the measurements are not affected by other noise sources in the system. It was also suggested that this technique could be used as a continuous stability monitor for a reactor system. A small amplitude input would be continually fed into the system. The impulsive response would be determined and displayed on an oscilliscope and thus any change toward instability could be noted.

Rajagopal (21) used a random external reactivity input to obtain the transfer function for a small reactor at Brookhaven National Laboratory. The random pulses from a radiation detector were converted to motion of a cadmium absorber located in the reactor. The input and output were crosscorrelated and Fourier transformed. The system transfer function was then obtained using Equation 31. It was reported that phase and magnitude data comparable to those obtained from oscillation tests were obtained.

Several papers on transfer function measurements and general reactor kinetics problems are presented in the proceedings of two reactor kinetics conferences (7, 8). Johnson (14) and Bloomfield and Bennett (5) have compiled extensive bibliographies on reactor kinetics.

IV. THEORY

A. Matrix Formulation of the Power Spectral Density Functions in a Linear System with Multiple Noise Sources

In any physical system the magnitudes of various parameters which describe the system may fluctuate around average values in a random manner. Also the system may be subjected to internally generated or externally applied random inputs. This leads one to consider the problem of describing the system behavior when it is subjected to multiple input noise sources. Moore (19) has studied this problem for a single region reactor and Wang and Uhlenbeck (29) have presented a general method of analysis connected with the study of Brownian motion. Leribaux (16) extended the work of Moore and introduced other noise sources which Moore neglected.

The general matrix formulation of an expression for the cross-power spectral density function between any two of the observable variables in a physical system is derived formally as follows.

The time behavior of a physical system, assumed to be described by n dependent variables, can be represented by n linear equations in the n variables. The general formulation is:

$$\begin{aligned} D_{11}\, x_1(t) + D_{12} x_2(t) + \ldots + D_{1n} x_n(t) &= f_1(t) \\ D_{21}\, x_1(t) + D_{22} x_2(t) + \ldots + D_{2n} x_n(t) &= f_2(t) \\ &\vdots \\ D_{n1}\, x_1(t) + D_{n2} x_2(t) + \ldots + D_{nn} x_n(t) &= f_n(t)\ , \end{aligned} \tag{32}$$

where

$D_{i,j}$ $(i_{i,j} = 1, 2, \ldots, n)$ are linear

combinations of differential operators of any order with respect to time;

$x_j(t)$ $(j = 1, 2, \ldots, n)$ is the jth dependent variable; and $f_i(t)$ is the ith input noise source. The variables $x_j(t)$ and $f_i(t)$ are assumed to be time stationary ergodic random functions.

The output correlation function is

$$\zeta_{i,j}(\xi) = \lim_{T\to\infty} \frac{1}{T} \int_{-T/2}^{T/2} x_i(t)\, x_j(t+\xi)\, dt, \tag{33}$$

$i_{i,j} = 1, 2, \ldots, n$

and the input correlation function is

$$\chi_{\ell m}(\xi) = \lim_{T\to\infty} \frac{1}{T} \int_{-T/2}^{T/2} f_\ell(t)\, f_m(t+\xi)\, dt. \tag{34}$$

$\ell, m = 1, 2, \ldots, n$

These correlation functions can be considered as the elements of two matrices, an input correlation matrix $[\chi]$ with elements $\chi_{\ell m}$ and an output matrix $[\zeta]$ with elements ζ_{ij}. In the frequency domain an output power spectral density matrix $[\Lambda]$ with elements

$$\Lambda_{ij}(\omega) = \int_{-\infty}^{\infty} \zeta_{ij}(\xi)\, e^{-j\omega\xi} d\xi, \tag{35}$$

and an input power spectral density matrix $[\Xi]$ with elements

$$\Xi_{\ell m}(\omega) = \int_{-\infty}^{\infty} \chi_{\ell m}(\xi)\, e^{-j\omega\xi} d\xi \tag{36}$$

can be defined.

Equation 33 is operated on with the differential operator $\overline{D_{pj}}$ which is the same as D_{pj} except that differentiation is taken with respect to ξ rather than t;

$$\overline{D_{pj}}\ \zeta_{ij}(\xi) = \lim_{T\to\infty} \frac{1}{T} \int_{-T/2}^{T/2} x_i(t)\ \overline{D_{pj}}\ x_j(t+\xi)\ dt. \tag{37}$$

A summation on the j index results in

$$\sum_{j=1}^{n} \overline{D_{pj}}\ \zeta_{ij}(\xi) = \lim_{T\to\infty} \frac{1}{T} \int_{-T/2}^{T/2} x_i(t) \left\{ \sum_{j=1}^{n} \overline{D_{pj}} x_j(t+\xi) \right\} dt. \tag{38}$$

The derivatives with respect to ξ in $\overline{D}_{pj}$ on the right side of Equation 38 can be replaced with derivatives with respect to $(t+\xi)$ since t and ξ are independent variables. The sum is then the same as the left side of Equation 32 with t replaced with $(t+\xi)$ so it follows that

$$\sum_{j=1}^{n} \overline{D}_{pj}\ x_j(t+\xi) = f_p(t+\xi)\ . \tag{39}$$

Substitution of Equation 39 into Equation 38 yields

$$\sum_{j=1}^{n} \overline{D}_{pj}\ \zeta_{ij}(\xi) = \lim_{T\to\infty} \frac{1}{T} \int_{-T/2}^{T/2} x_i(t)\ f_p(t+\xi)\ dt. \tag{40}$$

Equation 40 becomes

$$\sum_{j=1}^{n} \overline{D_{pj}}\ \zeta_{ij}(\xi) = \lim_{T\to\infty} \frac{1}{T} \int_{-T/2}^{T/2} f_p(\gamma)\ x_i(\gamma-\xi)\ d\gamma \tag{41}$$

with the change of variable $(\gamma = t + \xi)$ or

$$\sum_{j=1}^{n} \overline{D_{pj}}\ \zeta_{ij}(\xi) = \lim_{T\to\infty} \frac{1}{T} \int_{-T/2}^{T/2} f_p(t)\ x_i(t-\xi)\ dt \tag{42}$$

replacing γ with t.

It is now convenient to introduce the operators $\overline{D}_{ij}^{-}$ which are obtained by changing the signs of the derivatives of odd powers in $\overline{D}_{ij}$. Operation on Equation 42 with $\overline{D}_{qi}^{-}$ yields

$$\sum_{j=1}^{n} \overline{D}_{qi}^{-}\ \overline{D}_{pj}\ \zeta_{ij}(\xi) = \lim_{T\to\infty} \frac{1}{T} \int_{-T/2}^{T/2} f_p(t)\ \overline{D}_{qi}^{-}\ x_i(t-\xi)\ dt. \tag{43}$$

Summing on the i index results in

$$\sum_{i=1}^{n} \sum_{j=1}^{n} \bar{D}_{qi} \bar{D}_{pj} \zeta_{ij}(\xi) = \lim_{T\to\infty} \frac{1}{T} \int_{-T/2}^{T/2} f_p(t) \left\{ \sum_{i=1}^{n} \bar{D}_{qi} x_i(t-\xi) \right\} dt. \tag{44}$$

The derivatives with respect to ξ can be replaced with derivatives with respect to $(t-\xi)$ on the right side of Equation 44. Thus the sum on i is the same as Equation 32 with t replaced with $(t-\xi)$ and it follows

$$\sum_{i=1}^{n} \bar{D}_{qi} x_i(t-\xi) = f_q(t-\xi). \tag{45}$$

Substitution of Equation 45 into Equation 44 results in

$$\sum_{i=1}^{n} \sum_{j=1}^{n} \bar{D}_{qi} \bar{D}_{pj} \zeta_{ij}(\xi) = \lim_{T\to\infty} \frac{1}{T} \int_{-T/2}^{T/2} f_p(t) f_q(t-\xi) \, dt ,$$

or

$$= \lim_{T\to\infty} \frac{1}{T} \int_{-T/2}^{T/2} f_q(\mu) f_p(\mu+\xi) \, d\mu \tag{46}$$

with the change of variable $(\mu = t-\xi)$ or

$$= \lim_{T\to\infty} \frac{1}{T} \int_{-T/2}^{T/2} f_q(t) f_p(t+\xi) \, dt \tag{47}$$

since t is only a dummy variable of integration. Thus it follows

$$\sum_{i=1}^{n} \sum_{j=1}^{n} \bar{D}_{qi} \bar{D}_{pj} \zeta_{ij}(\xi) = \chi_{qp}(\xi) . \tag{48}$$

$$q \, p = 1, 2, \ldots, n$$

This is a system of n^2 linear differential equations in the $\zeta_{ij}(\xi)$. This system of differential equations can be changed to a system of n^2

algebraic equation by Fourier transforming both sides of Equation 48. The result is

$$\sum_{i=1}^{n} \sum_{j=1}^{n} \underline{D}_{qi}^{*} \underline{D}_{pj} \Lambda_{ij}(\omega) = \Xi_{qp}(\omega) \quad , \tag{49}$$

where:

$\underline{D}_{qi}^{*}$ is the complex conjugate of $\underline{D}_{qi}$ and is obtained from $\overline{\underline{D}}_{qi}$ by replacing $d/d\xi$ with $j\omega$;

$\underline{D}_{pj}$ is obtained from $\overline{\underline{D}}_{pj}$ by replacing $d/d\xi$ with $j\omega$; and $\Lambda_{ij}(\omega)$ and $\Xi_{qp}(\omega)$ are the output and input power spectral density functions defined by Equations 35 and 36. Equation 49 can be written in matrix form as

$$[\underline{D}^{*}] \cdot [\Lambda] \cdot [D^{T}] = [\Xi] \quad , \tag{50}$$

where $[\underline{D}^{T}]$ is the transpose of $[\underline{D}]$, that is $\underline{D}_{jp}^{T} = \underline{D}_{pj}$. If it is assumed that the [D] matrix has an inverse then it follows that

$$[\Lambda] = [\underline{D}^{*}]^{-1} \cdot [\Xi] \cdot [\underline{D}^{T}]^{-1} \tag{51}$$

so that

$$\Lambda_{\ell m}(\omega) = \sum_{i=1}^{n} \sum_{j=1}^{n} \underline{D}_{\ell i}^{*^{-1}} \Xi_{ij}(\omega) \underline{D}_{j\omega}^{T^{-1}} \quad , \tag{52}$$

or

$$\Lambda_{\ell m}(\omega) = \sum_{i=1}^{n} \sum_{j=1}^{n} (\underline{D}_{\ell i}^{-1})^{*} \underline{D}_{mj}^{-1} \Xi_{ij}(\omega) \quad . \tag{53}$$

Equation 53 follows from Equation 52 because

$$\underline{D}_{\ell i}^{*\,-1} = (\underline{D}_{\ell i}^{-1})^{*} \quad , \tag{54}$$

and

$$\underline{D}_{jm}^{T\,-1} = \underline{D}_{mj}^{-1} \quad . \tag{55}$$

The inverse $\underline{D}_{mj}^{-1}$ is found from

$$\underline{D}_{mj}^{-1} = \frac{\underline{d}_{jm}}{\text{det of } [\underline{D}]} \quad , \tag{56}$$

where:

$$d_{jm} = (-1)^{j+m} \left(\begin{array}{l} \text{det of matrix} \\ \text{without the} \\ \text{jth row and} \\ \text{mth column} \end{array} \right) . \qquad (57)$$

The quantity in parenthesis on the right side of Equation 57 is the minor D_{mj}.

Equation 53 can be used to find the power and cross power spectral density functions of all of the dependent variables in a system. This method of notation has the advantage that it can be applied in very complicated systems having multiple input noise functions.

B. Reactor Kinetics Equations for a Coupled Core System

The core of the UTR-10 reactor consists of two slightly subcritical slabs of fuel elements surrounded with graphite and separated by approximately 18 inches. The leakage interaction of neutrons between regions makes the two-slab system critical. This arrangement results in a possibility of semi-independent behavior of the two regions. It has been observed in the Argonaut reactor (2), which is also a two-fuel-region reactor, that the ratio of the average neutron fluxes in the two regions can be different from unity either during a transient condition or during equilibrium. This phenomenon is referred to as flux tilting.

The two-fuel-region system can be analyzed by considering each slab of fuel elements as a separate reactor system. The time behavior of each fuel region is described by a time dependent neutron diffusion equation. These equations differ from the usual form by the inclusion of a coupling term which accounts for the interaction effect of the opposite fuel region (9). The equations for region one are

$$\frac{dn_1(t)}{dt} = \frac{\Delta k_1}{\ell_1} n_1(t) - \frac{\beta}{\ell_1} n_1(t) + \sum_{i=1}^{6} \lambda_i C_{1i}(t) + \frac{\epsilon_1}{\ell_1} n_2(t-T) , \qquad (58)$$

$$\frac{dC_{1i}}{dt} = \frac{\beta_i}{\ell_1} n_1(t) - \lambda_i C_{1i}(t) , \qquad (59)$$

$$i = 1, 2, \ldots, 6$$

where:

$n_1(t)$ is the time dependent neutron density in region one, neutrons/cm^3;

$C_{1i}(t)$ is the delayed neutron precursor concentration for the ith group cm^{-3} and λ_i is the ith group decay constant; sec^{-1}, assumed to be the same in both regions;

Δk_1 is reactivity;

β_i is the delayed neutron fraction of the ith group with total fraction

β, assumed to be the same in both regions;

ℓ_1 is the prompt neutron lifetime, sec;

and $\frac{\epsilon_1}{\ell_1} n_2(t-T)$ accounts for the coupling effect of region two on one, ϵ_1 is the coupling reactivity and $n_2(t-T)$ is the neutron density in region two at some previous time (t-T) where T accounts for the time lag required for a disturbance to move between regions. The equations for region two are identical to those for region one with subscript 1 replaced by 2.

The delay time T was assumed by Baldwin (2) to be the time required for thermal neutrons (velocity of 2200 m/sec) to travel between regions. The delay time in this case is insignificant. A better approximation would be to assume that a neutron disturbance travels as a neutron wave with a frequency-dependent velocity. In this case the delay time is increased by a factor of ten but even then the delay time is quite insignificant except for very high frequencies. The frequency range considered in

this investigation is limited to 10 cps or less and in this case the delay time can be neglected without error.

It is convenient to replace the six groups of delayed neutrons with one group. With this approximation and neglecting the delay time T, the kinetics equations for the two regions can be written as

$$\frac{dn_1(t)}{dt} = \frac{\Delta k_1}{\ell_1} n_1(t) - \frac{\beta}{\ell_1} n_1(t) + \lambda C_1(t) + \frac{\epsilon_1}{\ell_1} n_2(t) , \tag{60}$$

$$\frac{dC_1(t)}{dt} = \frac{\beta}{\ell_1} n_1(t) - \lambda C_1(t) , \tag{61}$$

for region one and

$$\frac{dn_2(t)}{dt} = \frac{\Delta k_2}{\ell_2} n_2(t) - \frac{\beta}{\ell_2} n_2(t) + \lambda C_2(t) + \frac{\epsilon_2}{\ell_2} n_1(t) , \tag{62}$$

$$\frac{dC_2(t)}{dt} = \frac{\beta}{\ell_2} n_2(t) - \lambda C_2 , \tag{63}$$

for region two. For the one group approximation β_i is replaced by β, the total delayed fraction, and λ_i is replaced by a weighted average λ.

The object is to use Equations 60, 61, 62, and 63 along with Equation 53 to obtain the cross power spectral density function between the neutron densities of the two fuel regions of the UTR-10. During steady state operation $n_1(t)$ and $n_2(t)$ actually fluctuate around steady-state or average values under the influence of fluctuations of internal parameters such as absorption, fission, leakage, variations in coupling interactions, etc.

For purposes of the derivation it is convenient to express all of the time varying quantities as the sum of a steady state or average term and a small time dependent fluctuating term. The derivation will be carried out for region one and since the time-dependent diffusion equations

are of the same form the manipulations also apply to region two. The ratio of reactivity to lifetime will be fluctuating with time. This can be expressed by writing

$$\frac{\Delta k_1}{\ell_1} = H_{10} + h_1(t) \quad . \tag{64}$$

The zero subscript denotes the steady state condition. Also the multiplication of exchange neutrons will be time dependent so it follows

$$\frac{\epsilon_1}{\ell_1} = M_{10} + m_1(t) \quad . \tag{65}$$

It will be assumed that fluctuations in β/ℓ_1 can be neglected so that this can be written as

$$\frac{\beta}{\ell_1} = \frac{\beta_0}{\ell_0} = b \tag{66}$$

which corresponds to the steady state condition. The dependent variables also experience fluctuations;

$$n_1(t) = N_{10} + N_1(t) \quad , \tag{67}$$

$$C_1(t) = C_{10} + C_1(t) \quad . \tag{68}$$

Substitution of Equations 64, 65, 66, 67, and 68 into Equations 60 and 61 yields

$$\frac{dN_1(t)}{dt} = (H_{10} + h_1(t))(N_{10} + N_1(t)) - b\,(N_{10} + N_1(T)) + \lambda\,(C_{10} + C_1(t)) + (M_{10} + m_1(t))(N_{20} + N_2(t)) \quad , \tag{69}$$

and

$$\frac{dC_1(t)}{dt} = b(N_{10} + N_1(t)) - \lambda(C_{10} + C_1(t)) \quad , \tag{70}$$

or

$$\frac{dN_1(t)}{dt} = H_{10}N_1(t) + h_1(t)\,N_{10} - bN_1(t) + \lambda C_1(t) + m_1(t)N_{20} + M_{10}N_2(t) \tag{71}$$

and

$$\frac{dC_1(t)}{dt} = bN_1(t) - \lambda C_1(t) , \tag{72}$$

where products of fluctuations have been neglected and sums of steady state terms have been eliminated to obtain Equations 71 and 72. These equations can be rewritten as

$$(\frac{d}{dt} - H_{10}+b)N_1(t) - \lambda C_1(t) - M_{10}N_2(t) = h_1(t)N_{10} + M_1(t)\, N_{20}, \tag{73}$$

and

$$-b\, N_1(t) + (\frac{d}{dt} + \lambda)\, C_1(t) = 0. \tag{74}$$

It will be assumed that the steady state coupling coefficient is the same for each region and also the average value of the prompt neutron lifetime since both fuel regions are approximately identical. It is convenient to introduce the notation

$$\begin{aligned} \underline{P} &= \frac{d}{dt} \quad , \qquad F = \frac{N_{20}}{N_{10}} \\ M_{10} &= M_{20} = \frac{\epsilon_o}{\ell_o} = a, \; b = \frac{\beta}{\ell_o} \\ H_{10} &= \frac{\Delta k_o}{\ell_o} = -\frac{\epsilon_o}{\ell_o} F = -aF, \quad (9) \\ H_{20} &= \frac{\Delta k_o}{\ell_o} = -\frac{\epsilon_o}{\ell_o F} = -\frac{a}{F} \qquad (9) \quad . \end{aligned} \tag{75}$$

With this notation the system of equations for the two core reactor becomes

$$(\underline{P} + aF + b)\, N_1(t) - aN_2(t) - \lambda\, C_1(t) + 0 = f_1(t) , \tag{76}$$

$$-b\, N_1(t) + 0 + (\underline{P} + \lambda)C_1(t) + 0 = f_2(t) , \tag{77}$$

$$-aN_1(t) + (\underline{P} + \frac{a}{F} + b)\, N_2(t) + 0 - \lambda C_2(t) = f_3(t) , \tag{78}$$

$$+0 - b\, N_2(t) + 0 + (\underline{P} + \lambda)\, C_2(t) = f_4(t) \quad , \tag{79}$$

where:

$$f_1(t) = h_1(t)\, N_{10} + m_1(t)\, N_{20} \tag{80}$$

$$f_2(t) = f_4(t) = 0 \tag{81}$$

$$f_3(t) = h_2(t)\, N_{20} + m_2(t)\, N_{10} \quad . \tag{82}$$

Matrix notation can be used to express the system of Equations 76 through 79;

$$[D] \cdot [X] = [f] \, , \tag{83}$$

where:

$$[D] = \begin{bmatrix} \underline{P} + aF + b & -\lambda & -a & 0 \\ -b & \underline{P} + \lambda & 0 & 0 \\ -a & 0 & \underline{P} + \frac{a}{F} + b & -\lambda \\ 0 & 0 & -b & \underline{P} + \lambda \end{bmatrix} , \tag{84}$$

and

$$[X] = \begin{bmatrix} N_1(t) \\ C_1(t) \\ N_2(t) \\ C_2(t) \end{bmatrix} , \qquad [F] = \begin{bmatrix} f_1(t) \\ f_2(t) \\ f_3(t) \\ f_4(t) \end{bmatrix} \quad . \tag{85}$$

This system of equations is of the same form as the general set of Equation 32.

Equation 53 is now used to find the cross power spectral density function between the dependent variables $N_1(t)$ and $N_2(t)$;

$$\Lambda_{13}(\omega) = (\underline{D}_{11}^{-1})^* \, \underline{D}_{31}^{-1} \, \Xi_{11}(\omega) + (\underline{D}_{13}^{-1})^* \, \underline{D}_{33}^{-1} \, \Xi_{33}(\omega) \quad . \tag{86}$$

Equation 86 follows from Equation 53 because all input power spectral density functions, other than $\Xi_{11}(\omega)$ and $\Xi_{33}(\omega)$, are zero either because

the other input functions are uncorrelated or zero. Leribaux (16) has shown that

$$\Xi_{11}(\omega) = N_{10}\ \frac{1}{\ell_o}^{*} + N_{20}\ a\ , \tag{87}$$

where:

$$\frac{1}{\ell_o}^{*} = \frac{1}{\ell_o}\left(\frac{\bar{\nu}^2 - \bar{\nu}}{\bar{\nu}}\right)$$

and $\dfrac{\bar{\nu}^2 - \bar{\nu}}{\bar{\nu}} = 1.96$

$\bar{\nu}$ is the average number of neutrons produced per fission, and

$$\Xi_{33}(\omega) = N_{10}\left(F\ \frac{1}{\ell_o}^{*} + a\right). \tag{88}$$

From Equation 56;

$$\underline{D}_{mj}^{-1} = \frac{\underline{d}_{jm}}{\text{det of } [\underline{D}]}\ , \tag{89}$$

$\underline{d}_{jm}$ is the cofactor (j, m) of $[\underline{D}]$ and this is found from the matrix [D] by replacing $\underline{P}$ with $j\omega$. For the UTR-10 b is of the order of 20 and λ is approximately 0.08 therefore λ will be neglected.

With the substitution of Equation 89 into Equation 86, the cross power spectral density function becomes

$$\begin{aligned}\Lambda_{13}(\omega) &= \frac{\underline{d}_{11}^{*}}{\det\ [\underline{D}]^{*}}\ \frac{\underline{d}_{13}}{\det\ [\underline{D}]}\ \Xi_{11}(\omega) \\ &\quad + \frac{\underline{d}_{31}^{*}}{\det\ [\underline{D}]^{*}}\ \frac{\underline{d}_{33}}{\det\ [\underline{D}]}\ \Xi_{33}(\omega)\ , \\ &= \frac{\underline{d}_{11}^{*}\ \underline{d}_{13}}{|\det\ [\underline{D}]|^2}\ \Xi_{11}(\omega) + \frac{\underline{d}_{31}^{*}\ \underline{d}_{33}}{|\det\ [\underline{D}]|^2}\ \Xi_{33}(\omega)\ ,\end{aligned} \tag{90}$$

and det $[\underline{D}]$ is

$$\det\ [\underline{D}] = \left|\begin{bmatrix} j\omega+aF+b & -\lambda & -a & 0 \\ -b & j\omega+\lambda & 0 & 0 \\ -a & 0 & j\omega+\frac{a}{F}+b & -\lambda \\ 0 & 0 & -b & j\omega+\lambda \end{bmatrix}\right|$$

$$= -\lambda b \left[(j\omega + \frac{a}{F} + b)(j\omega + \lambda) - \lambda b\right]$$

$$+ (j\omega + \lambda) \left\{ -a^2(j\omega+\lambda)+(j\omega+aF+b) \left[(j\omega+ \frac{a}{F} + b)(j\omega+\lambda) - \lambda b\right]\right\} . \quad (91)$$

With the assumption of $\lambda \ll b$, det $[\underline{D}]$ becomes

$$\det [\underline{D}] = j\omega \left[(j\omega)^3 + (j\omega)^2(aF + \frac{a}{F} + 2b)\right.$$

$$+ j\omega (b^2 + \frac{ab}{F} + abF)$$

$$\left. + \lambda ab (\frac{1}{F} + F)\right] . \quad (92)$$

This can be factored as

$$\det [\underline{D}] = j\omega (j\omega+b) \left[(j\omega)^2 + j\omega (aF + \frac{a}{F} + b) + \lambda a (\frac{1}{F} + F)\right] \quad (93)$$

which introduces an extra term $j\omega\lambda a (\frac{1}{F} + F)$ but with the assumption of small λ this term is negligible compared to the term $j\omega ab (\frac{1}{F} + F)$.

The determinant can be further factored into

$$\det [\underline{D}] = j\omega (j\omega + b)(j\omega + F'a + b)(j\omega + \frac{F'a\lambda}{F'a+b}) , \quad (94)$$

where the substitution $\frac{1}{F} + F = F'$ has been made. The absolute magnitude of the determinant is obtained by multiplying Equation 94 by the complex conjugate;

$$|\det [\underline{D}]|^2 = \omega^2 (\omega^2 + \omega_1^2)(\omega^2 + \omega_2^2)(\omega^2 + \omega_3^2) , \quad (95)$$

where

$$\omega_1 = b$$

$$\omega_2 = F'a + b$$

$$\omega_3 = \frac{F'a\lambda}{F'a+b} .$$

The cofactors have to be evaluated next. From Equation 84 it follows that $\underline{d}_{11}^*$ is

$$\underline{d}_{11}^* = \left| \begin{bmatrix} -j\omega + \lambda & 0 & 0 \\ 0 & -j\omega + \frac{a}{F} + b & -\lambda \\ 0 & -b & -j\omega + \lambda \end{bmatrix} \right|$$

$$= (-j\omega + \lambda) \left[\frac{a\lambda}{F} - \omega^2 - j\omega \left(\frac{a}{F} + b\right)\right] , \tag{96}$$

and $\underline{d}_{13}$

$$\underline{d}_{13} = \begin{vmatrix} -b & j\omega + \lambda & 0 \\ -a & 0 & -\lambda \\ 0 & 0 & j\omega + \lambda \end{vmatrix}$$

$$= a\,(j\omega + \lambda)^2 . \tag{97}$$

Similarly,

$$\underline{d}_{31}^{*} = \begin{vmatrix} -\lambda & -a & 0 \\ -j\omega + \lambda & 0 & 0 \\ 0 & -b & -j\omega + \lambda \end{vmatrix}$$

$$= a(-j\omega + \lambda)^2 . \tag{98}$$

Then $\underline{d}_{33}$ is found from

$$\underline{d}_{33} = \begin{vmatrix} j\omega + aF + b & -\lambda & 0 \\ -b & j\omega + \lambda & 0 \\ 0 & 0 & j\omega + \lambda \end{vmatrix}$$

$$= (j\omega + \lambda) [\lambda aF - \omega^2 + j\omega (aF + b)] . \tag{99}$$

Substitution of Equations 87, 88, 95, 96, 97, and 98 into Equation 90 yields

$$\Lambda_{13}(\omega) = a\, N_{10}\left(\frac{1}{\ell_o}' + Fa\right) \frac{(\omega^2 + \lambda^2) \left\{ (j\omega + \lambda) \left[\frac{a\lambda}{F} - \omega^2 - j\omega \left(\frac{a}{F} + b\right)\right]\right.}{\omega^2 (\omega^2 + \omega_1^2)(\omega^2 + \omega_2^2)(\omega^2 + \omega_3^2)}$$

$$\left. + \frac{C\,(-j\omega + \lambda)[\lambda aF - \omega^2 + j\omega (aF + b)]}{\omega^2 (\omega^2 + \omega_1^2)(\omega^2 + \omega_2^2)(\omega^2 + \omega_3^2)} \right\} , \tag{100}$$

where

$$C = \frac{F \frac{1}{\ell_o}' + a}{\frac{1}{\ell_o}' + Fa} .$$

The factor F accounts for flux tilting between the two cores. It has been shown that F ranges between 0.95 and 0.84 (9). During the

experimental measurements the value was maintained approximately at the maximum by control rod positioning. In this case the flux tilting effect will be quite small and negligible error will be introduced if F is taken as one.

For purposes of calculation and comparison with experimental data values of ω greater than one will be considered. In this case Equation 100 can be further simplified to the form

$$\Lambda_{13}(\omega) = a\, N_{10} \left(\frac{1}{\ell_o}' + a\right) \omega^2 \left\{ \frac{j\omega\,[a\lambda - \omega^2 - j\omega\,(a+b)]}{\omega^2(\omega^2+\omega_1^2)(\omega^2+\omega_2^2)(\omega^2+\omega_3^2)} \right.$$

$$\left. \frac{-j\omega\,[\lambda a - \omega^2 + j\omega\,(a+b)]}{\omega^2\,(\omega^2+\omega_1^2)(\omega^2+\omega_2^2)(\omega^2+\omega_3^2)} \right\}$$

$$= \frac{k^1}{(\omega^2+\omega_1^2)(\omega^2+\omega_2^2)} \quad . \tag{101}$$

Thus the cross-power spectral density function is a real quantity. A small phase angle would actually be present due to flux tilting and the time delay required for a disturbance to move between the fuel regions. It was found from exploratory calculations that the phase lag is approximately constant at 2 degrees over the range of frequencies from 0.5 to 10 cps. Equation 100 expresses the cross power spectral density function for frequencies above one radian per second. The significant features of this expression are the two corner frequencies at ω_1 and ω_2. By comparing the theoretical curve obtained from the equation with the experimental data the best values for the parameters ℓ_o and ϵ_o can be estimated.

V. EXPERIMENTAL EQUIPMENT AND TECHNIQUES

The equipment and experimental techniques used in the investigation are described in this section.

A. Reactor

The noise measurements were carried out in the Iowa State University UTR-10 reactor[1] which is a modified, commercial version of the Argonaut reactor developed at Argonne National Laboratory. The core of the UTR-10 consists of two 5 in. by 20 in. by 24 in. subcores, each containing approximately 72 MTR-type fuel elements surrounded by graphite and cooled and moderated by deionized light water. This arrangement provides for an internal graphite reflector between the fuel regions. Five removable stringers are provided with access to the stringers available through openings in the top shield closures. A thermal column 4 ft. by 5 ft. by 5 ft. long is also provided. An access port to the midplane of the south fuel region can be obtained by removing the central graphite stringer in the thermal column.

The reactor is fueled by approximately 3 kg of U-235 in the form of fully enriched (greater than 93%) uranium. The fuel loading in the form of uranium-aluminum fuel elements is divided approximately equally between the two fuel regions. The maximum licensed power level of the reactor is 10 kw and at this power the maximum thermal neutron flux is approximately 2×10^{11} neutrons/cm^2-sec.

The reactor is controlled by means of two safety rods, one regulating

---

[1] A product of Advanced Technology Laboratories, a Division of American Standard, Mountain View, California.

rod and one shim-safety rod. During operation the safety rods are fully withdrawn. The shim-safety rod is situated near the north core tank and the regulating rod is located by the south core tank.

Locations of stringer positions used in this investigation as well as other pertinent features of the UTR-10 are shown in Figure 5.

B. Noise Measuring Equipment

Basically the experimental methods used in this study consisted of the following steps: (1) the outputs from two ion chambers positioned near the two fuel regions of the UTR-10 were displayed on a dual beam oscilloscope and recorded on 35 mm movie film; (2) both traces on the film were sampled in 1/120 second intervals; and (3) the correlation and power spectral functions were then calculated on an IBM 7074. Further details of equipment and procedures used are presented in the following sections.

The reactor noise was detected by means of RCL[1] model 10511 BF_3 detectors operated as ion chambers. A typical high voltage-current characteristic curve for these chambers is shown in Figure 6. The operating voltage was chosen as 1200 volts for all runs. A conventional scalar was used as a high voltage supply.

It was found that there was a large amount of 60-cycle pickup from the chambers and leads. To eliminate this, each chamber was wrapped in a plastic sheet and then the chamber and leads were wrapped in heavy aluminum foil which was grounded to the common ground of the system. This

---

[1] A Product of Radiation Counter Laboratories, Inc., Skokie, Illinois.

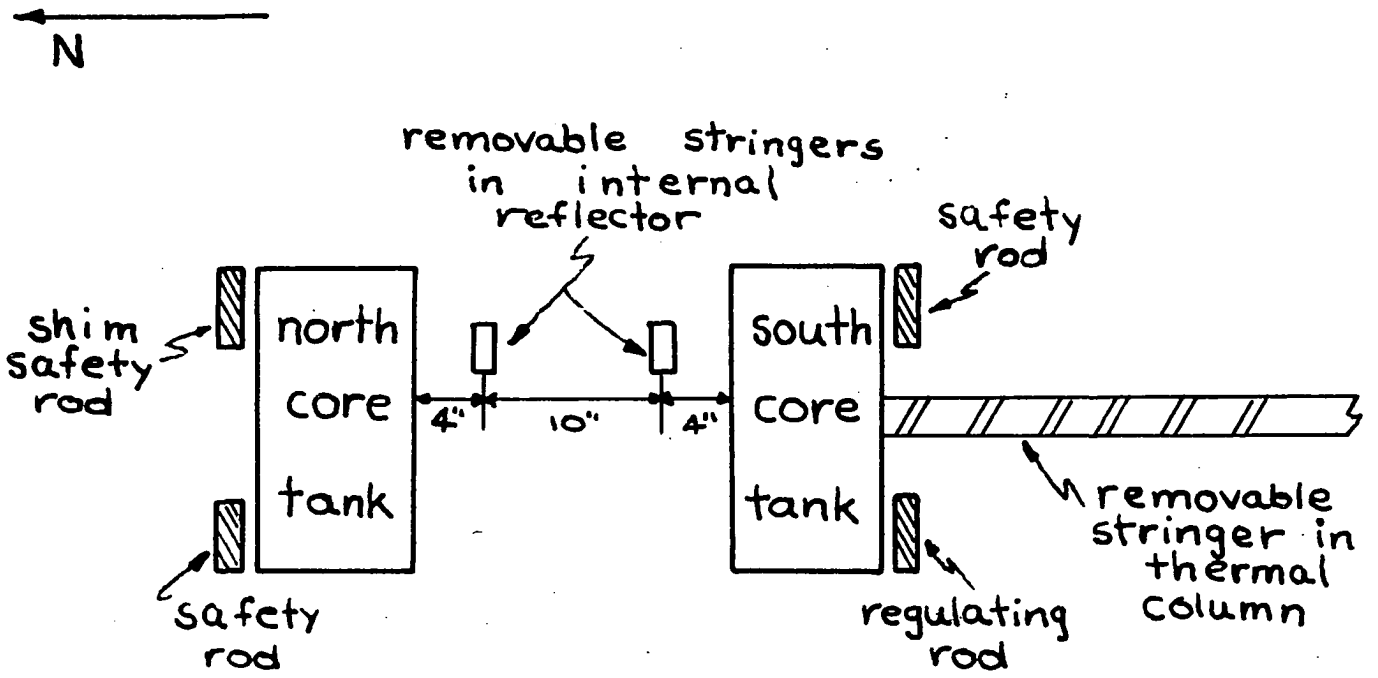

Figure 5. Plan view of UTR-10 showing important features

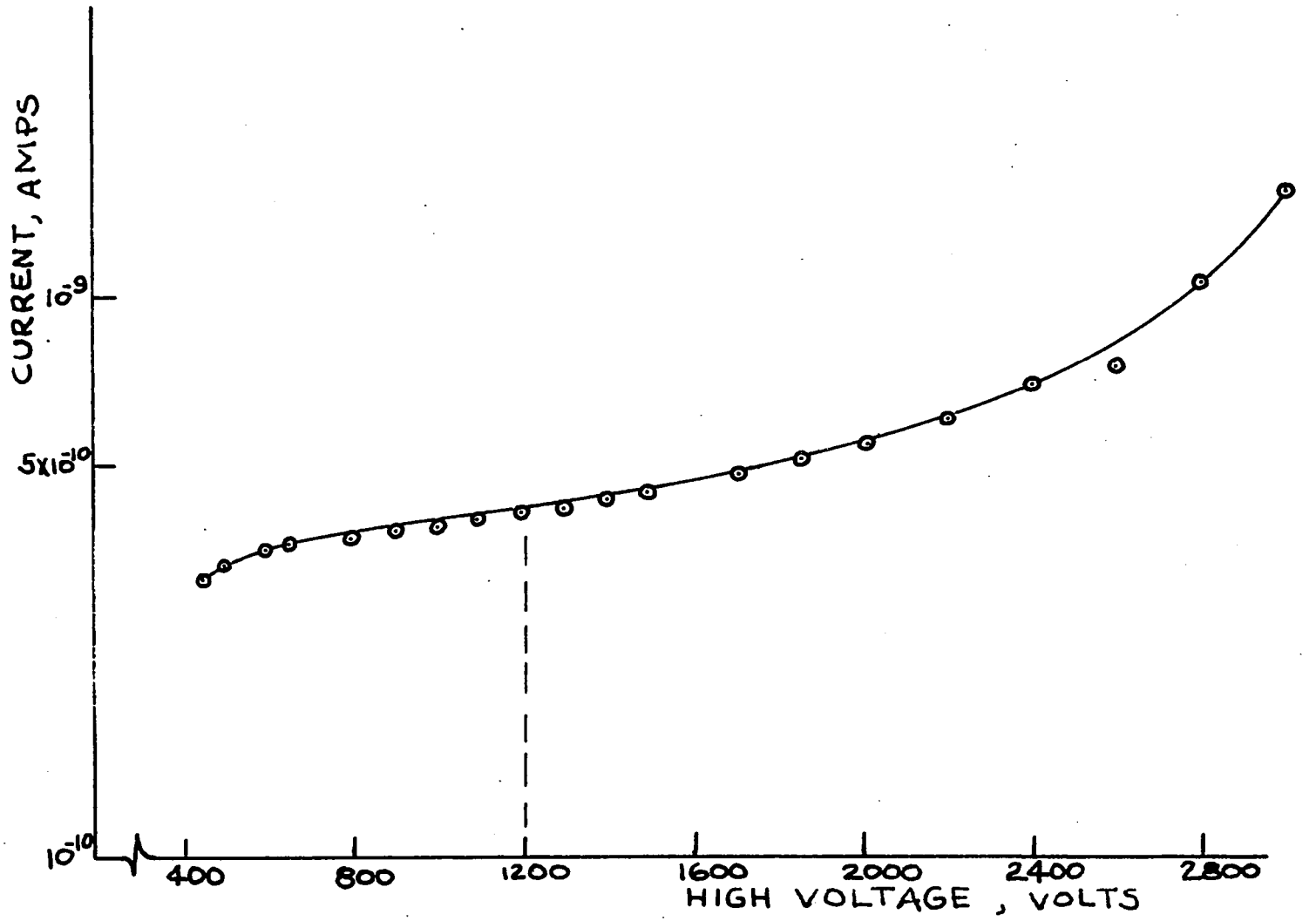

Figure 6. Voltage-current characteristics of BF_3 detector

was found to be quite effective in eliminating 60-cycle hum from the signals from the chambers.

The output current from each ion chamber was fed into a Keithley[1] micro-microammeter where the current fluctuations were converted to a time varying voltage. The Keithley model 610 was used for one channel and the model 410 for theother. The main difference between the two models is that the model 610 can also be used as a volt meter or ohm meter. Also, the A.C. noise level in the model 410 was found to be much larger than in the model 610. To reduce this noise the power supply in the ammeter was replaced with external, well filtered, high voltage power supplies for the B+ and a six-volt storage battery for the tube filaments. The output from the micro-microammeter was then passed through a band pass filter to remove undesirable low frequency fluctuations such as slow reactor drift and also to reduce the 60-cycle noise and higher frequency tube noise that might be present. A Krohn-Hite[2] ultra low frequency band pass filter model 330A was used in one channel and a band pass filter was simulated on a Donner[3] analog computer for the other channel. The high and low pass settings were 0.02 cps and 40 cps for all runs. The wiring diagram for the analog computer is shown in Figure 7. The experimentally measured high frequency response for this filter is shown in Figure 8. The input is attentuated by 10 db at 60 cps.

The output from each measuring channel was then displayed on a

---

[1]A product of Keithley Instruments, Inc., Cleveland, Ohio.

[2]A product of Krohn-Hite Corporation, Cambridge, Mass.

[3]A product of Donner Scientific Company, A division of Systron-Donner Corporation, Concord, California.

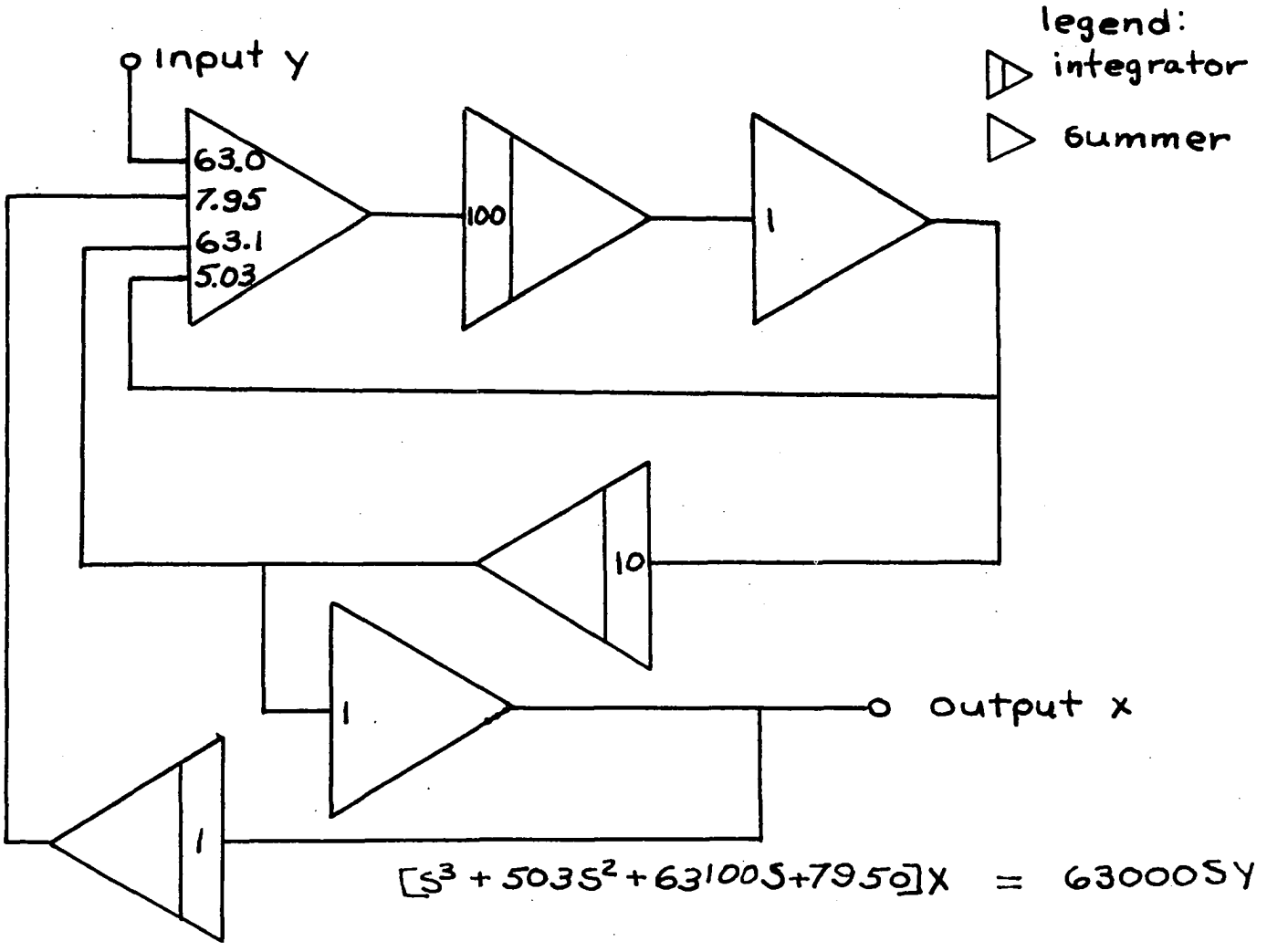

Figure 7. Analog computer wiring diagram of simulated band pass filter

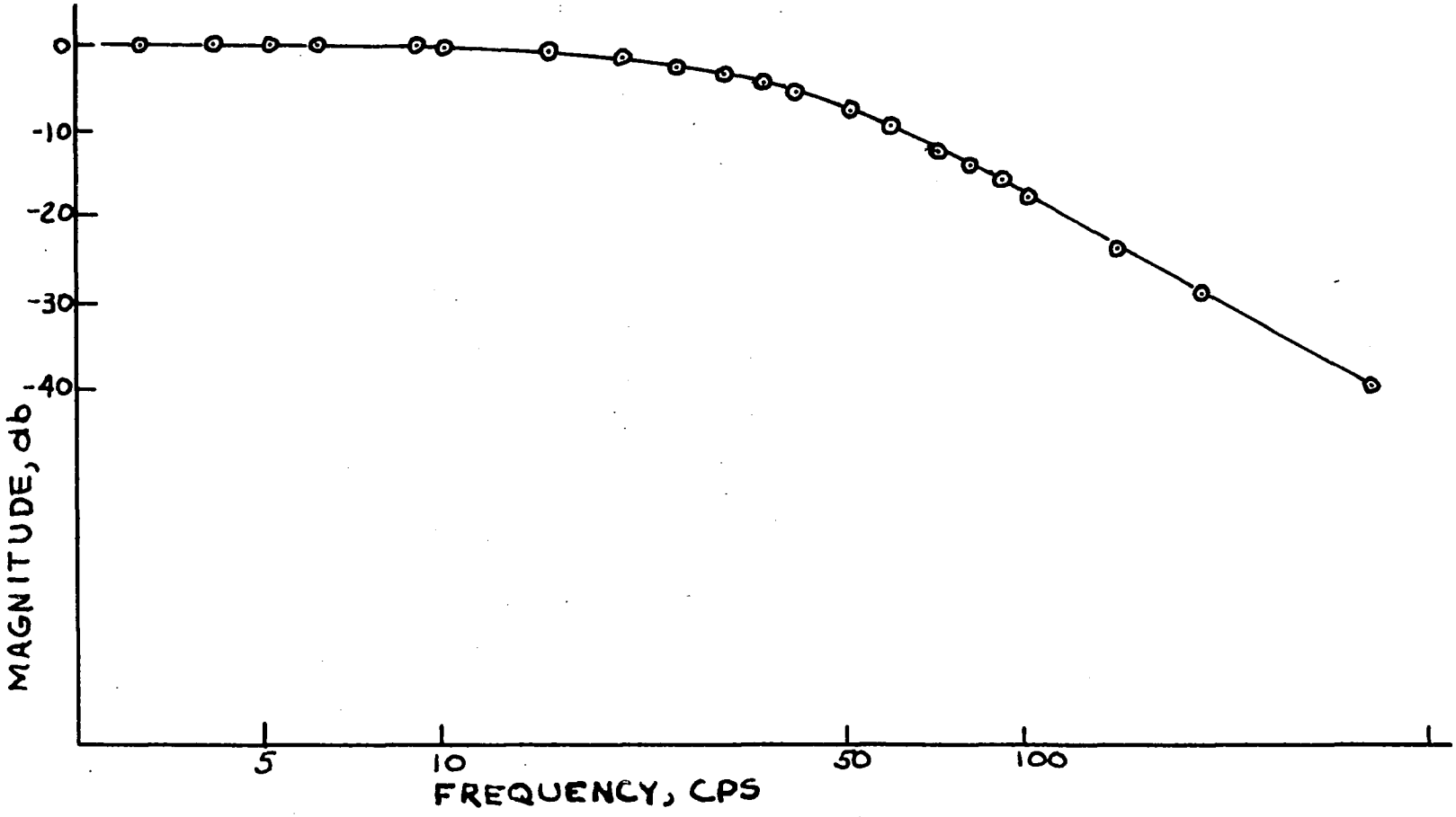

Figure 8. Frequency response of simulated band pass filter

Tektronix[1] dual beam type 502 oscilloscope. A DuMont[2] oscillosgraph record camera type 321 was used to record the reactor signals. The time sweep of the oscilloscope was not activated so that only two vertical traces were obtained on the screen. The film moving at 1200 inches per minute provided the time base. A shielded neon bulb was attached to the oscilloscope screen in the field of the camera to produce timeing dots on the film.

A conventional micro-film reader was used to project the film on graph paper with a magnification of approximately twenty.

A diagram of the arrangement of the experimental equipment is shown in Figure 9.

C. Experimental Procedures

The experimental techniques used in the investigation are discussed in this section.

Two crosscorrelation runs were made. In run number 1 the two ion chambers were located in the graphite between the cores in the openings provided by removing the small stringers shown in Figure 5. Each chamber was located at the approximate midplane of the reactor, 4 inches from a fuel region. In run number 2 the north slab chamber was located in the same position as for run number 1 and the south region chamber was positioned in the thermal column against the south face of the south fuel region. The south chamber was positioned in the central stringer position in the thermal column as shown in Figure 5.

---

[1] A product of Tektronix, Inc., Portland, Oregon.

[2] A product of Allen B. DuMont Laboratories, Inc., Clifton, New Jersey.

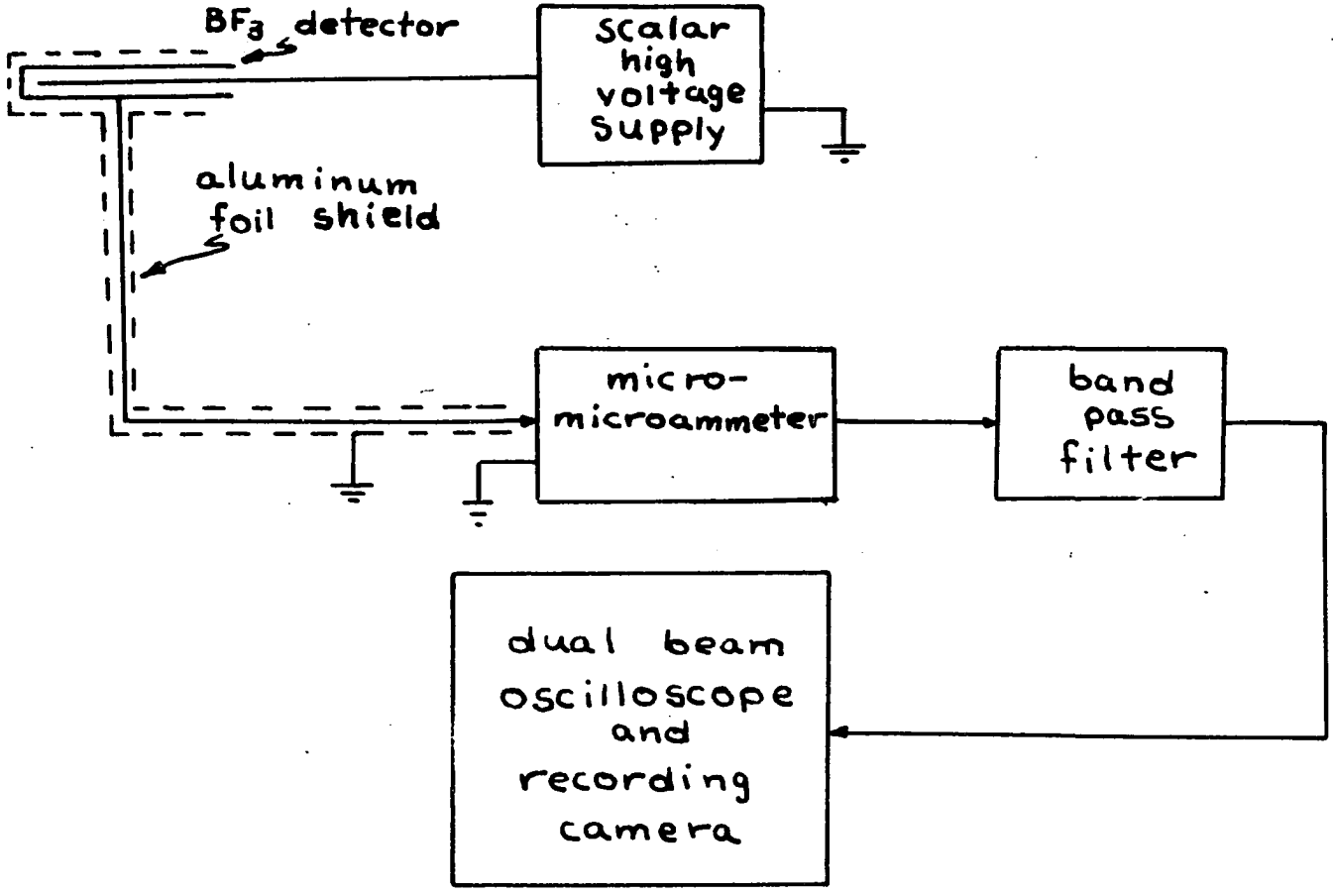

Figure 9. Equipment block diagram

During each run the reactor was left on manual control. Care was taken to insure that the reactor power level was not drifting while data was being taken. The reactor power for both runs was 0.04 watts.

Data were taken for approximately 12 seconds for each run. It was desired to sample at least ten seconds of the reactor signal as this seemed to represent a reasonable compromise between accuracy and length of sample.

Leribaux (16) has shown that a 10-second sampling time results in a maximum standard deviation of approximately 6% for this system.

Typical sections of the records from runs 1 and 2 are shown in Figure 10. The timing dots are 1/60 of a second apart. The film records were sampled in 1/120 second intervals by interpolating between dots. Thus a ten-second run resulted in 1200 observations from each trace. A voltage polarity change was experienced in the analog computer which accounts for the apparent 180-degree phase shift between the two signals. This inversion caused no difficulty in the analysis and merely resulted in a sign change in the cross correlation functions.

D. Analysis of Data

The experimental measurements of correlation and power spectral density functions must be based on finite observation times. Thus, the measured functions are approximations to the ideal functions. The difference between the measured and ideal relationships depends upon several things, two of the more important being sampling time and the characteristics of the physical system. For example, a five-second sampling interval might be quite adequate for an autocorrelation measurement in a system having a time constant of 0.01 second but it would

Figure 10. Sections of film records

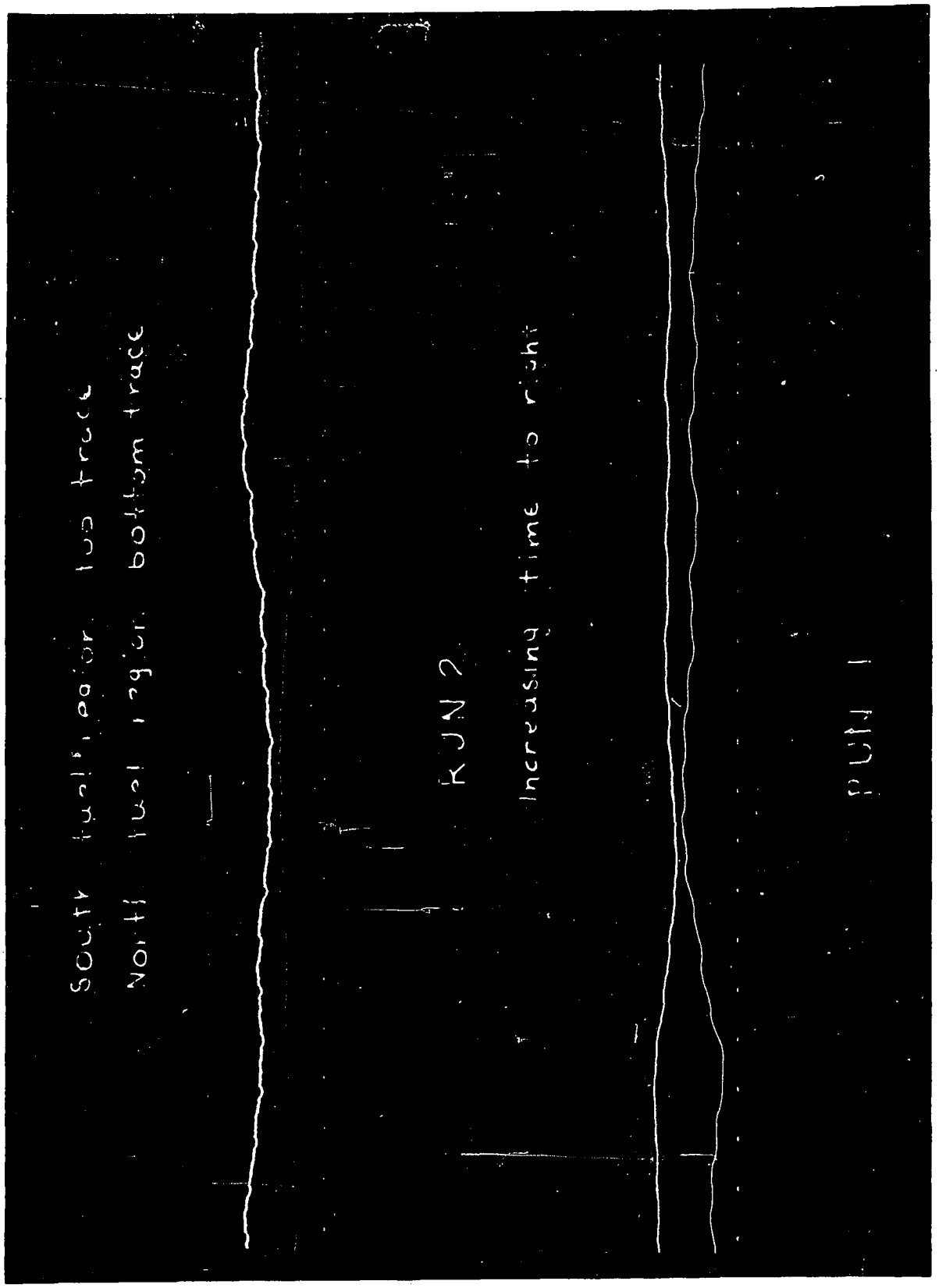
South fuel region top trace
North fuel region bottom trace
RUN 2
Increasing time to right
RUN 1

be inadequate for a system with a 100-second time constant.

Two different techniques might be used to determine the experimental power spectral functions. A theoretical mathematical expression could be fitted to the experimental correlation functions by a method of least squares and then substituted into the appropriate expression, Equations 15 or 27, or the experimental data could be used directly in a numerical analysis. The latter method was used in this investigation. An alternate method for measuring these functions directly is discussed in Appendix C.

The data read from the film were used to calculate the crosscorrelation functions. The correlation functions, $\zeta_{xy}(\xi)$, were approximated by the average lagged products calculated from the expressions

$$\zeta_{xy}(-\xi) = \frac{1}{N} \sum_{i=1-Lag}^{N} (X_i - \bar{X})(Y_{i+Lag} - \bar{Y}) \quad , \tag{102}$$

for negative lags or

$$\zeta_{xy}(\xi) = \frac{1}{N} \sum_{i=1}^{N-Lag} (X_i - \bar{X})(Y_{i+Lag} - \bar{Y}) \tag{103}$$

for positive lags. If x = y an autocorrelation function is obtained and if $x \neq y$ a crosscorrelation function is obtained. The average of the set of observations X_i or Y_i is $\bar{X}$ or $\bar{Y}$. The averages are subtracted out so the final expressions are for data with zero average. The total number of observation is N. There is some question as to the correct value to use for N. Prazen (20) points out that if N is taken as the total number of observations and this value is used for calculating all $\zeta_{xy}(\pm \xi)$ the mean square error of $\zeta_{xy}(\pm \xi)$ as an estimate of the true correlation function is less than that obtained if $(N \pm Lag)$ is used. In other words it is best to make no correction in the calculation of

the average lagged products for the data lost from the end of the series. In most cases the difference between the two methods is not significant except for large lags.

For purposes of machine calculations Equations 102 and 103 were rewritten as

$$\zeta_{xy}(-\xi) = \frac{N\sum_{i=1-Lag}^{N} X_i Y_{i+Lag} - \sum_{i=1}^{N} Y_i \sum_{i=1-Lag}^{N} X_i - \sum_{i=1}^{N} X_i \sum_{i=1-Lag}^{N} y_{i+Lag} + \frac{\sum_{i=1}^{N} X_i \sum_{i=1}^{N} Y_i \left(\frac{N+Lag}{N}\right)}{N^2}}{N^2}, \quad (104)$$

and

$$\zeta_{xy}(\xi) = \frac{N\sum_{i=1}^{N-Lag} X_i Y_{i+Lag} - \sum_{i=1}^{N} Y_i \sum_{i=1}^{N-Lag} X_i - \sum_{i=1}^{N} X_i \sum_{i=1}^{N-Lag} Y_{i+Lag} + \frac{\sum_{i=1}^{N} X_i \sum_{i=1}^{N} Y_i \left(\frac{N-Lag}{N}\right)}{N^2}}{N^2}. \quad (105)$$

The cross power spectral density function was obtained from the relationship

$$\Lambda_{xy}(\omega) = \sum_{r=-Lag}^{Lag} \zeta_{xy}(r) \left[\cos r\omega - j \sin r\omega\right], \quad (106)$$

where $\zeta_{xy}(r)$ is obtained from Equation 104 or 105 for the appropriate lag. The program was also written to calculate the frequency distribution of observations about the mean. The Fortran Statements for the IBM 7074 programs are given in Appendix B.

VI. RESULTS

The crosscorrelation functions for runs 1 and 2 are shown in Figures 11 and 12 respectively, and numerical values are tabulated in Appendix A Tables 3 and 4. The data for each run were normalized to the product of the root mean square values of the two random functions (σ, the standard deviation) making up the respective crosscorrelation functions. The results indicate that for approximately zero lag the neutron outputs of the south and north cores are 85 per cent correlated in the case of run 1 and 77 per cent correlated for run 2. Also, the crosscorrelation functions approach zero for increasing values of lag. These results are reasonable from a physical standpoint. Since the two fuel regions are coupled the maximum correlation should occur at approximately zero lag. It also seems reasonable to expect the degree of correlation to decrease with increased lag since for a stable system the behavior at the present time should be approximately independent of events occurring in the infinite past.

The statistical nature of the random functions representing the neutron fluctuations in the two cores is illustrated in Figure 13. The probability density function of the distribution of amplitudes for the output of the south core for run 1 is plotted versus the amplitude. A normal or Gaussian probability density function P(x) given by

$$P(x) = \frac{1}{\sigma (2\pi)^{1/2}} \exp \left[-\tfrac{1}{2} \frac{(x-\mu)^2}{\sigma^2} \right] , \qquad (107)$$

where:

σ is the standard deviation (A value of 41.6 was used)

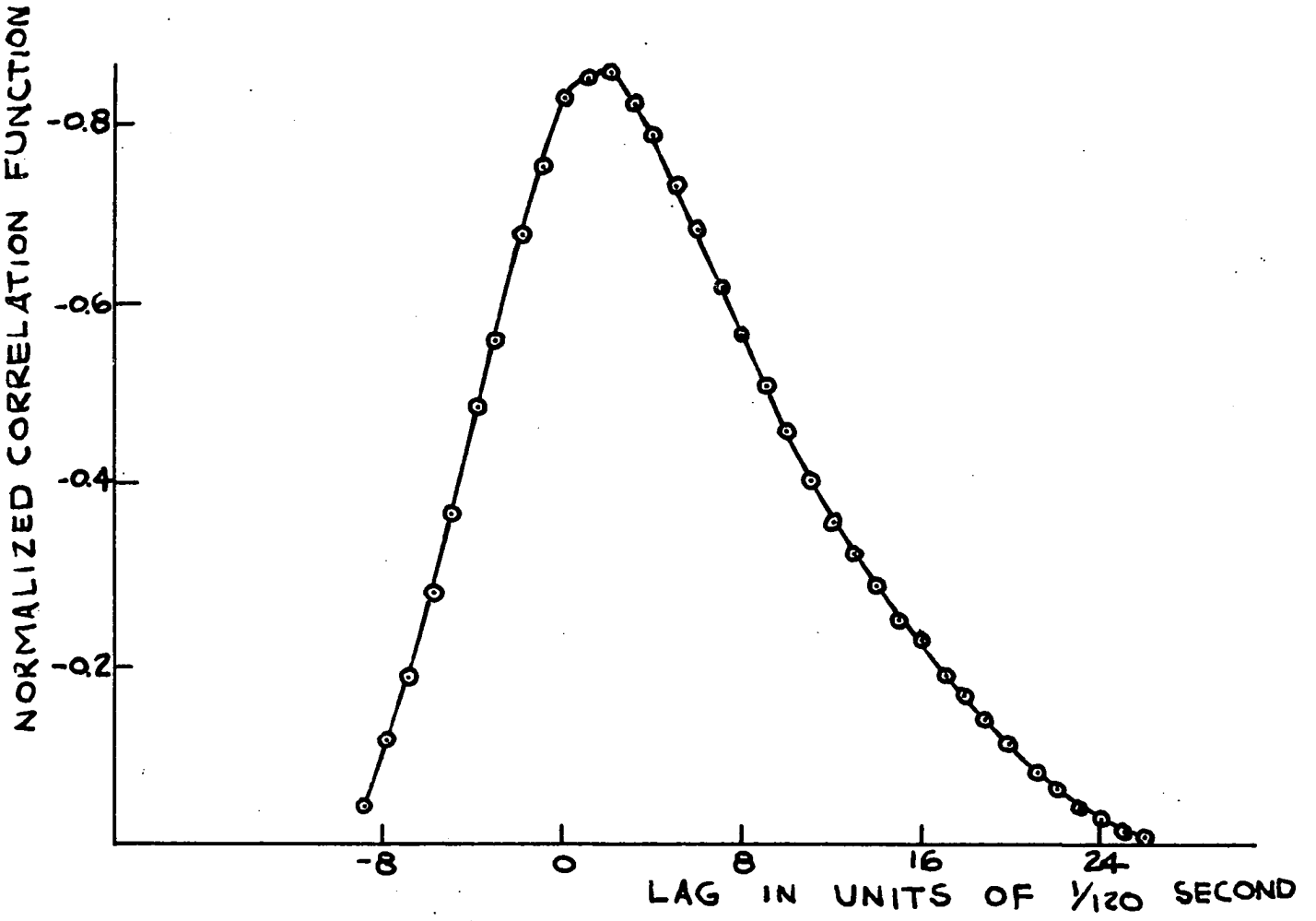

Figure 11. Crosscorrelation function for run 1

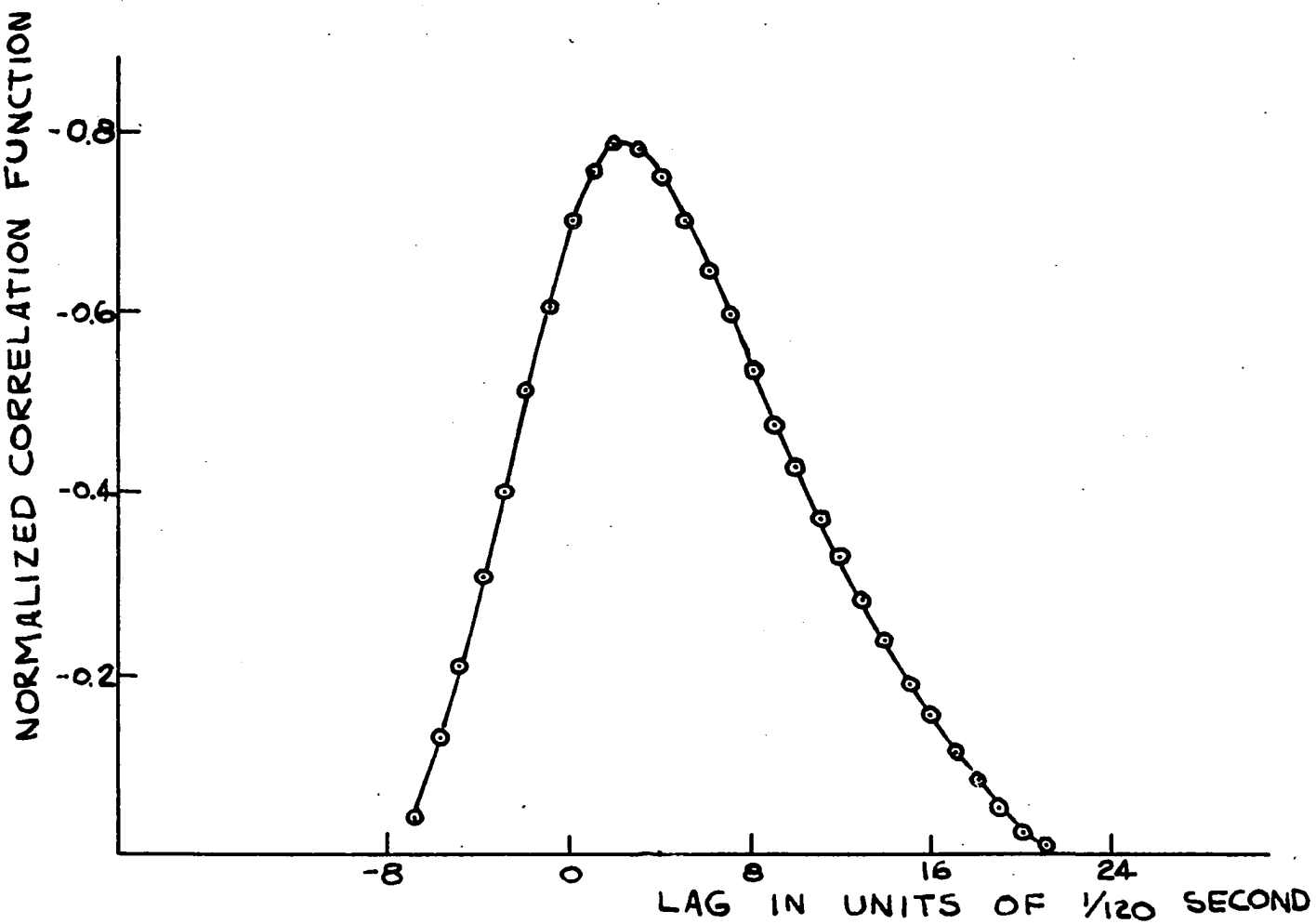

Figure 12. Crosscorrelation function for run 2

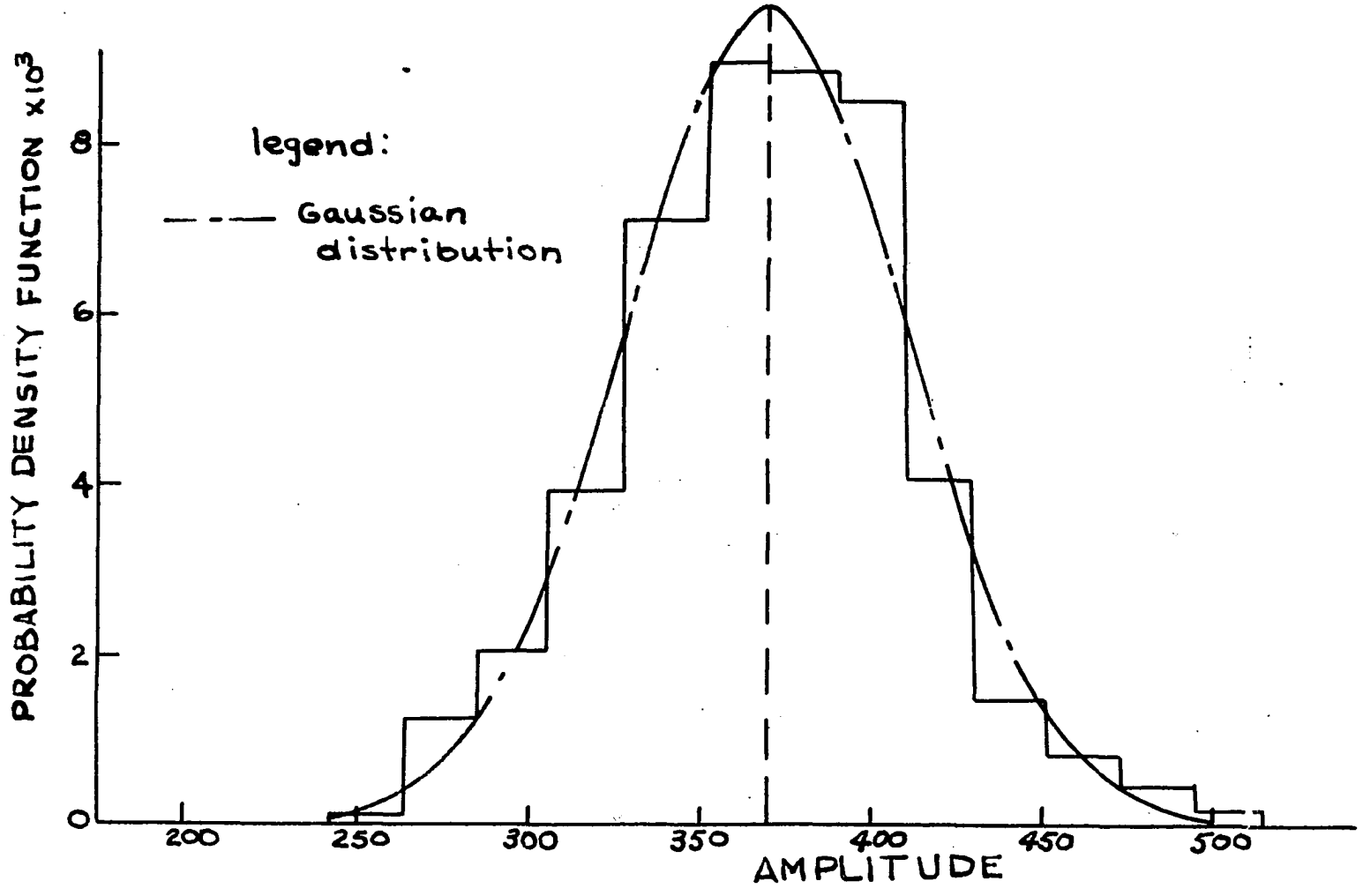

Figure 13. Distribution of amplitudes

μ is the mean of the random variable. (The mean for this case was 369)

x is the amplitude of the random function

is plotted on the same curve. It is apparent that the experimental data follow a normal distribution quite closely. The comparison is summarized in Table 1.

Table 1. Statistical comparison

Percent of Observations	Greater than mean	Within $\pm$ 0.674 σ	Within $\pm\sigma$	Within $\pm$ 2σ
Gaussian Distribution	50	50	68.2	95.4
Experimental Observations	50.2	51.2	70.6	94.4

The crosscorrelation functions were transformed by means of Equation 106 to obtain the cross-power spectral functions. The magnitudes of the experimental cross power spectral functions expressed in db (db = 20 $\log_{10}$ magnitude) and normalized to 1 cps are presented in Figures 14 and 15 for runs 1 and 2 respectively. Numerical values are presented in Appendix A Tables 5 and 6.

It was shown in Section IV that the theoretical cross power spectral function, $\Lambda_{13}(\omega)$, between the outputs of the two fuel regions of the coupled core reactor system is given by

$$\Lambda_{13}(\omega) = \frac{k^1}{(\omega^2 + \omega_1^2)(\omega^2 + \omega_2^2)} \quad , \tag{108}$$

where:

$$\omega_1 = \frac{\beta}{\ell_o}$$

$$\omega_2 = 2\frac{\epsilon_o}{\ell_o} + \frac{\beta}{\ell_o} \quad ,$$

for Φ greater than 1 radian per second. The best estimates of k^1, ω_1 and ω_2 were obtained by the method of least squares. For purposes of calculation it is convenient to take the logarithim of both sides of Equation 108 and then minimize the function

$$G = \sum_{i=1}^{N} \left\{ \ln k^1 - \ln (\omega_i^2 + \omega_1^2) - \ln (\omega_i^2 + \omega_2^2) - \ln \bar{\Lambda}_{13}(\omega_i) \right\}^2, \quad (109)$$

where $\bar{\Lambda}_{13}(\omega_i)$ is the normalized experimental value of the cross power spectral function for $\omega = \omega_i$. The requirement that the G function be a minimum imposes the condition that the partial derivatives of G with respect to the parameters k^1, ω_1 and ω_2 be zero, therefore

$$\frac{\partial G}{\partial k} = 0 = \sum_{i=1}^{N} \left\{ \ln k^1 - \ln (\omega_i^2 + \omega_1^2) - \ln (\omega_i^2 + \omega_2^2) - \ln \bar{\Lambda}_{13}(\omega_i) \right\} , \quad (110)$$

$$\frac{\partial G}{\partial \omega_1} = 0 = \sum_{i=1}^{N} \left\{ \ln k^1 - \ln (\omega_i^2 + \omega_1^2) - \ln (\omega_i^2 + \omega_2^2) - \ln \bar{\Lambda}_{13}(\omega_i) \right\} \frac{1}{\omega_i^2 + \omega_1^2} \quad , \quad (111)$$

$$\frac{\partial G}{\partial \omega_2} = 0 = \sum_{i=1}^{N} \left\{ \ln k^1 - \ln (\omega_i^2 + \omega_1^2) - \ln (\omega_i^2 + \omega_2^2) - \ln \bar{\Lambda}_{13}(\omega_i) \right\} \frac{1}{\omega_i^2 + \omega_2^2} \quad . \quad (112)$$

The theoretical curves for the values of k^1, ω_1 and ω_2 obtained from the least square fit are also shown in Figures 14 and 15. The best values for k^1, ω_1 and ω_2 for both runs are tabulated in Table 2 along with the corresponding values of ℓ_o and ϵ_o for an effective delayed neutron fraction β of 0.007. This value, which is greater than the total fraction of delayed neutrons, 0.0064, has been shown to be appropriate

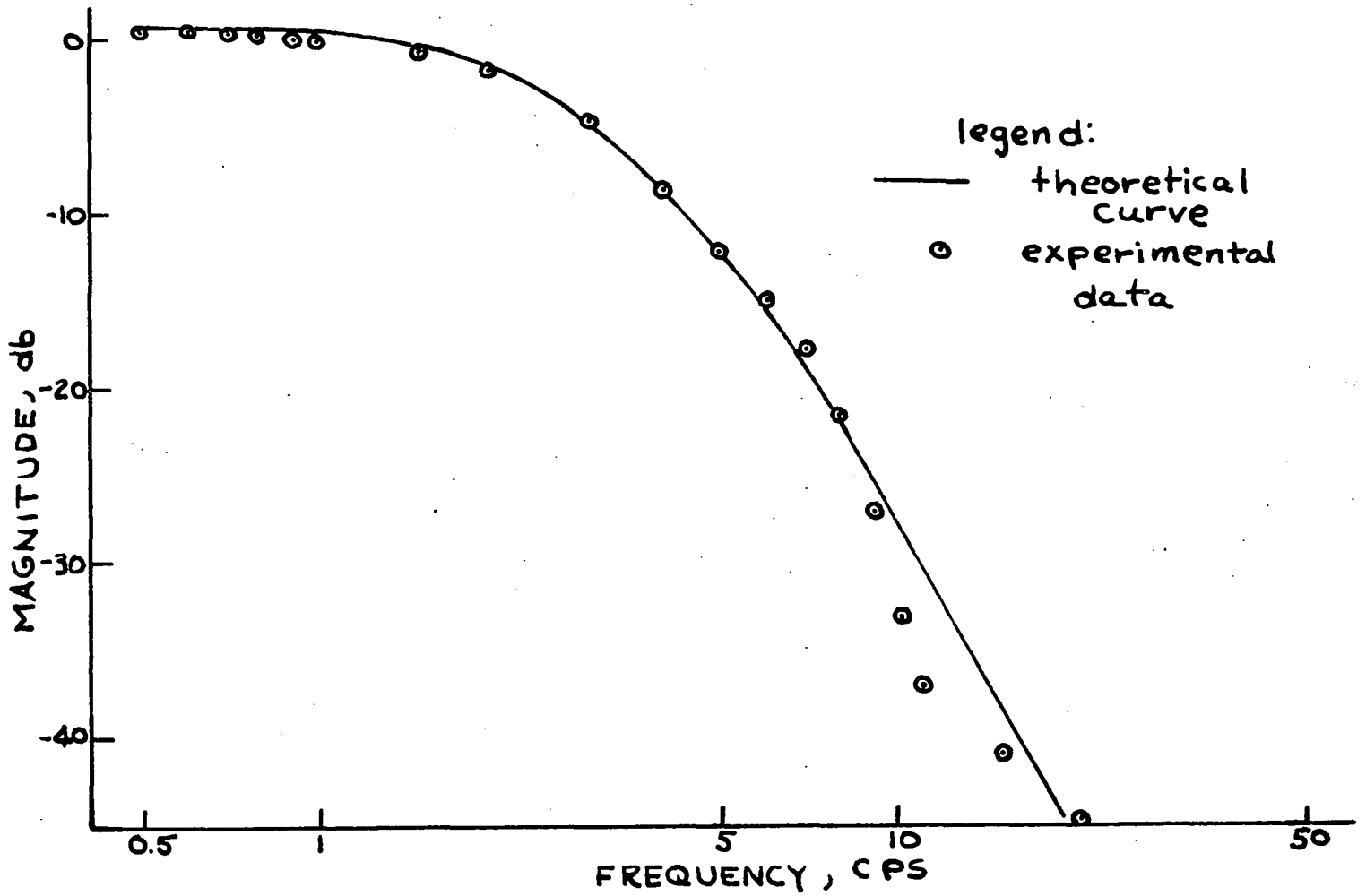

Figure 14. Cross power spectral density function for run 1

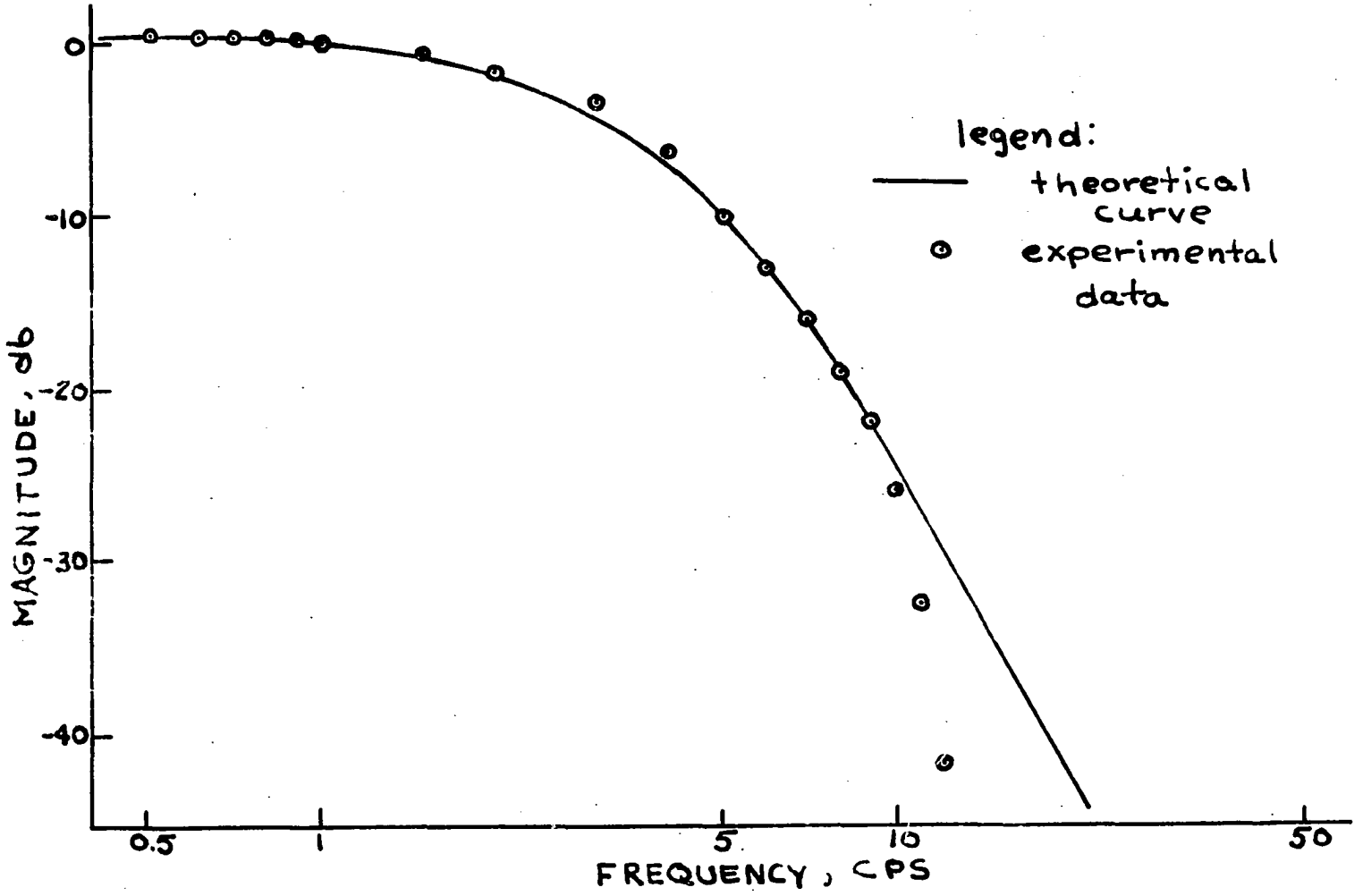

Figure 15. Cross power spectral density function for run 2

for an Argonaut-type reactor.

The slope of the experimental cross power spectral density function appears to increase more rapidly beyond approximately 9 cps in the case of run 1 and 10.0 cps for run 2. It was felt that data for higher frequencies were questionable so cross power spectral values for frequencies greater than those indicated were neglected in the curve fitting. The increased slope may indicate a loss of correlation.

Table 2. Tabulation of results

	ω_1, rad/sec	ω_2, rad/sec	k^1, rad^2/sec^2	ϵ_o	ℓ_o, sec
Run 1	17.5	58.1	1.36×10^6	0.00789	0.000400
Run 2	23.0	57.0	2.02×10^6	0.00517	0.000304

The neutron lifetime ℓ_o for both runs is larger than the value calculated by the designer of the reactor (1.35×10^{-4} seconds) but it is in good agreement with the value of 3.41×10^{-4} seconds measured by Leribaux. The value of neutron lifetime reported for the UTR-10 is based upon a one-dimensional two-group approximation and inaccuracies in this calculation may account for the discrepancy between the measured and calculated values.

The coupling coefficient of reactivity between regions, ϵ_o, has been reported as 1.55×10^{-2} for the UTR-10.[1] This value is larger than the coupling coefficients measured in this work but it is of the same order of

[1]Crews, Ray F. Mountain View, California. Reactivity data. Private communication to Dr. Glenn Murphy. 1959.

magnitude. The reported value was obtained from estimates of the amount of fuel required to make the single slab reactor critical. This was obtained by extrapolating reciprocal counting rate data obtained during a critical experiment. The reactivity worth of the required additional fuel was obtained from the average mass coefficient of reactivity for the reactor. It is felt that the uncertainties present in the measurement of the reported coupling coefficient could certainly account for the differences observed here. In either case the results serve to indicate that the two cores of the UTR-10 are quite loosely coupled, that is the value of K_{eff} is quite close to one for each fuel region; 0.992 for run number 1, 0.994 for run 2 and 0.9845 for the reported value. The difference in the three values of K_{eff} is quite small. It is felt that the results obtained from run 2 should yield the best estimates of the parameters involved since for this run the chambers were positioned so that shadowing effects between the fuel regions would be minimized.

VII. CONCLUSIONS

The major conclusions to be drawn from the investigation are as follows:

(1) The cross correlation function is a smooth function of the lag with a maximum at approximately zero lag and it decreases quite rapidly with increasing positive or negative lag.

(2) The cross power spectral density function between the neutron fluxes in the two core regions is approximately constant over a limited range of frequencies and the higher frequency components are attenuated quite rapidly beyond a cutoff frequency of approximately 3 cps.

(3) A method of measuring the reactivity coupling between regions is developed. The results obtained serve to indicate that the two fuel regions of the UTR-10 are loosely coupled, that is K_{eff} for each region is quite close to unity (0.992 - 0.9845).

(4) It has been demonstrated that a relatively simple recording technique can be used for obtaining cross-correlation measurements. Inexpensive equipment can be used although the experimental work is quite lengthy.

(5) The experimental data fit the theoretical cross power spectral function quite closely over the range of frequencies investigated. The maximum deviation is less than 2 db.

VIII. SUGGESTIONS FOR FUTURE WORK

There are many areas for future research in the application of random noise theory to the study of reactor kinetics. A partial list of some of the more obvious is as follows:

(1) Direct cross power spectral density measurements using the techniques described in Appendix C.

(2) Crosscorrelation measurements between other variables in the system (neutron density and temperature, control rod motion, etc.).

(3) Development of a magnetic tape recording system for autocorrelation and crosscorrelation measurements.

(4) Crosscorrelation measurements between a programmed random reactivity noise input and neutron density.

(5) Crosscorrelation measurements between the neutron density fluctuations in various regions of the reactor.

(6) Subcritical reactor noise measurements to obtain shut down margins.

IX. LITERATURE CITED

1. Balcomb, Douglas J., Demuth, Howard B., and Gyftopoulos, Elias P. A crosscorrelation method for measuring the impulsive response of reactor systems. Nuclear Science and Engineering. 11:159-166. 1961.

2. Baldwin, G. C. Kinetics of a reactor composed of two loosely coupled cores. Nuclear Science and Engineering. 6:320-327. 1959.

3. Batch, M.L. and Ball, R. M. Use of noise analysis to measure reactor stability on N. S. Savannah. American Nuclear Society Transactions 5, No. 1:175. 1962.

4. Bendat, Julius S. Principles and applications of random noise theory. New York, N.Y., John Wiley and Sons, Inc. 1958.

5. Bloomfield, M. and Bennett, F. G. Reactor kinetics: a bibliography. U. S. Atomic Energy Commission Report NAA-SR-3808 [North American Aviation, Inc. Downey, California]. 1959.

6. Cohn, C. E. Determination of reactor kinetic parameters by pile noise analysis. Nuclear Science and Engineering. 5:331-335. 1959.

7. Conference on Transfer Function Measurements and Reactor Stability Analysis Proceedings. U.S. Atomic Energy Commission Report ANL-6205 [Argonne National Laboratory, Lemont, Illinois]. 1960.

8. Conference on Reactor Kinetics Proceedings, 1960. U.S. Atomic Energy Commission Report IDO-16791 [Idaho Operations Office]. 1960.

9. Danofsky, R. A. Kinetic behavior of coupled reactor cores. Unpublished M.S. thesis. Ames, Iowa, Library, Iowa State University of Science and Technology. 1960.

10. DeShong, J. A. Power transfer functions of the EBWR obtained using a sinusoidal reactivity driving function. U.S. Atomic Energy Commission Report ANL-5798 [Argonne National Laboratory, Lemont, Illinois]. 1958.

11. DeShong, J. A. Upping EBWR's power. Nucleonics. 16, No. 6:68-72. June 1958.

12. Griffin, C. W. and Lundholm, J. G. Measurement of the SRE and KEWB prompt neutron lifetime using random noise and reactor oscillator techniques. U.S. Atomic Energy Commission Report NAA-SR-3765 [North American Aviation, Inc. Downey, California]. 1959.

13. Harrer, J. M., Boyer, R. E., and Kuucoff, Darwin. Transfer function of Argonne CP-2 reactor. Nucleonics. 10, No. 8:32-36. Aug. 1952.

14. Johnson, R. L. Kinetics, stability, and control a selected bibliography. U.S. Atomic Energy Commission Report NAA-SR-7786 [North American Aviation, Inc. Downey, California]. 1963.

15. Kasten, P. R. HRT transfer function information. U.S. Atomic Energy Commission Report IDO-16791:161-170. [Idaho Operations Office]. 1960.

16. Leribaux, H. R. Stochastic processes in coupled nuclear reactor cores. Unpublished Ph.D. thesis. Ames, Iowa, Library, Iowa State University of Science and Technology. 1963.

17. Luckow, W. K. Predicting reactor temperature excursions by extrapolating Borax data. Nucleonics. 14, No. 1:23-25. Jan. 1956.

18. Moore, M. N. The determination of reactor transfer functions from measurements at steady operation. Nuclear Science and Engineering. 3:387-394. 1958.

19. Moore, M. N. The power noise transfer function of a reactor. Nuclear Science and Engineering. 6:448-452. 1959.

20. Prazen, E. An approach to time series analysis. The Annals of Mathematical Statistics. 32:951-989. 1961.

21. Rajagopal, V. Determination of the reactor transfer function by statistical correlation methods. Nuclear Science and Engineering. 12:218-224. 1962.

22. Savant, C. J., Jr. Basic feedback control system design. New York, N.Y., McGraw-Hill Book Co., Inc. 1958.

23. Schultz, M. A. Control of nuclear reactors and power plants. 2nd ed. New York, N.Y., McGraw-Hill Book Co., Inc. 1961.

24. Skinner, R. E. and Hetrick, D. L. The transfer function of a water boiler reactor. Nuclear Science and Engineering. 3:573-594. 1958.

25. Thie, J. A. Operating information from reactor noise. Nucleonics. 21, No. 3:72-75. March 1963.

26. Thie, J. A. Statistical analysis of power reactor noise. Nucleonics. 17, No. 10:102-111. Oct. 1959.

27. Uhrig, R. E. Random variations of neutron density in a subcritical assembly. American Nuclear Society Transactions 4, No. 1:85. 1961.

28. Ulrich, A. J. Results of recent analysis of Borax II transient experiments. U.S. Atomic Energy Commission Report ANL-5532 [Argonne National Laboratory, Lemont, Illinois]. 1956.

29. Wang, M. C. and Uhlenbeck, G. E. On the theory of brownian motion. II. Reviews of Modern Physics. 17:323-342. 1945.

30. Zinn, W. H. Experimental investigation of the self-limitation of power during reactivity transients in a sub-cooled, water moderated reactor, Borax I experiments. U.S. Atomic Energy Commission report ANL-5323 [Argonne National Laboratory, Lemont, Illinois]. 1954.

X. ACKNOWLEDGMENTS

The author wishes to express his gratitude to his major professor, Dr. Glenn Murphy, head of the Nuclear Engineering Department, for by his encouragement, advice and understanding the years of graduate study were made more profitable and enjoyable; and who also by his professional attainments has always presented a challenge to strive to reach higher goals of professional development. Acknowledgments are also due for nuclear reactor time and equipment furnished which made the present work possible.

It is also a pleasure to express appreciation to the National Science Foundation for its help in the form of a Graduate Faculty Fellowship.

Acknowledgment is also due to the computation center for computer time obtained for unsponsored research.

XI. APPENDIX A

A. Tabulation of Experimental Data

Table 3. Crosscorrelation data run 1, where M = 1/120 second, σ_x = 80.3, σ_y = 41.6[a]

ξ (sec)	$-\zeta_{xy}(\xi)$	$-\frac{\zeta_{xy}(\xi)}{\sigma_x \sigma_y}$[b]
-9M	132.5454	0.0396
-8M	378.7383	0.114
-7M	608.7535	0.1821
-6M	919.2881	0.275
-5M	1204.4019	0.361
-4M	1557.2844	0.465
-3M	1868.3294	0.559
-2M	2222.1487	0.665
-1M	2491.6170	0.746
0	2740.1161	0.821
1M	2827.4706	0.847
2M	2849.6774	0.853
3M	2733.1681	0.819
4M	2616.9600	0.783
5M	2423.0549	0.725
6M	2264.2539	0.679
7M	2049.5724	0.614
8M	1887.9343	0.565
9M	1681.8360	0.505
10M	1534.6504	0.460
11M	1349.4951	0.404
12M	1229.1361	0.367
13M	1070.9782	0.322
14M	972.6190	0.291
15M	832.3172	0.249
16M	750.0802	0.224

[a] σ_x is the standard deviation of north core data and σ_y is the standard deviation of south core data.

[b] Rounded off to three significant figures to be consistent with accuracy of input data.

Table 3 (Continued)

ξ (sec)	$-\zeta_{xy}(\xi)$	$-\frac{\zeta_{xy}(\xi)}{\sigma_x \sigma_y}$
17M	624.2912	0.187
18M	554.0352	0.166
19M	436.8814	0.131
20M	371.7356	0.111
21M	262.0090	0.0785
22M	212.9461	0.0635
23M	126.3258	0.0377
24M	100.3644	0.0299
25M	29.8709	0.0089
26M	10.0557	0.0030

Table 4. Crosscorrelation data run 2, where M = 1/120 seconds, $\sigma_x = 40.8$, $\sigma_y = 42.7$

ξ (sec)	$-\zeta_{xy}(\xi)$	$-\frac{\zeta_{xy}(\xi)}{\sigma_x \sigma_y}$
-7M	85.1705	0.0490
-6M	213.9657	0.123
-5M	355.3128	0.204
-4M	520.2523	0.299
-3M	690.0845	0.396
-2M	868.7994	0.499
-1M	1031.6016	0.594
0M	1183.9800	0.681
1M	1289.2433	0.741
2M	1342.2551	0.772
3M	1329.5712	0.764
4M	1281.2328	0.738
5M	1197.6501	0.688
6M	1106.7094	0.635
7M	1003.7877	0.577
8M	906.7589	0.522
9M	807.9388	0.465
10M	722.4222	0.415
11M	634.9461	0.364
12M	560.8661	0.323
13M	482.5949	0.277
14M	412.7603	0.238
15M	334.0136	0.192
16M	267.0686	0.154
17M	198.1567	0.114
18M	142.7234	0.0821
19M	86.7959	0.0499
20M	47.1240	0.0271
21M	6.6923	0.00385

Table 5. Cross power spectral data run 1

Frequency (cps)	Magnitude	db-(db)[a], cps
0.5	45212.121	+0.425
0.6	44901.758	+0.342
0.7	44537.484	+0.258
0.8	44120.541	+0.172
0.9	43652.355	+0.0800
1.0	43134.515	0
1.5	39867.254	-0.690
2.0	35682.387	-1.66
3.0	25961.705	-4.44
4.0	16916.448	-8.14
5.0	10814.851	-12.0
6.0	7729.133	-14.9
7.0	5695.331	-17.6
8.0	3648.983	-21.5
9.0	1924.019	-27.1
10.0	984.656	-33.0
11.0	526.221	-37.4
12.0	208.293	-46.5
15.0	389.498	-41.0
20.0	238.931	-45.0

[a]Rounded off to three significant figures to be consistent with accuracy of input data.

Table 6. Cross power spectral data run 2

(Frequency) cps	Magnitude	db-(db), cps
0.5	18901.730	+0.300
0.6	18810.501	+0.270
0.7	18703.168	+0.170
0.8	18579.970	+0.170
0.9	18441.183	+0.0800
1.0	18287.116	0
1.5	17300.626	-0.465
2.0	15996.310	-1.16
3.0	12727.593	-3.12
4.0	9153.729	-6.02
5.0	5970.070	-9.70
6.0	3735.871	-13.8
7.0	2615.470	-16.9
8.0	2093.800	-18.9
9.0	1584.223	-21.2
10.0	987.382	-25.4
11.0	488.934	-32.2
12.0	121.140	-43.6

XII. APPENDIX B

A. Fortran Statements

1. Correlation function

```
    1    DIMENSION X(2000,2),C(18)
    1    DIMENSION X(2000,2),C(18)
         COMMONX
    2    FORMAT (2I4,18F4.0)
    3    FORMAT (2I1,I4,3I3,2F3.1)
  100    FORMAT (I5,E20.8)
  101    FORMAT (5E20.8)
  102    FORMAT (1H,2I5,I6,3I5,2F5.1)
  103    FORMAT (2I5,18F6.0)
    5    READ3,L,M,N,LAGL,LAGU,LAGDEC,F,D
    6    PRINT102,L,M,N,LAGL,LAGU,LAGDEC,F,D
   10    READ2,ID1,ID2,(X(I,L),I=1.18)
   11    PRINT103,ID1,ID2,(X(I,L),I=1,18)
   12    IF(ID2-1)13,14,13
   13    STOP89
   14    IJ=N-18
         DO21I=18,IJ,18
   15    READ2,ID11,ID22,(C(K),K=1,18)
   16    PRINT103,ID11,ID22,(C(K),K=1,18)
   17    IF(ID11-ID1)13,18,13
   18    IF(ID22-ID2-1)13,19,13
   19    ID2=ID22
         DO21K=1,18
   20    J=I+K
   21    X(J,L)=C(K)
   22    IF(M-1)23,30,23
   23    IF(M-2)24,27,24
   24    IF(M)13,25,13
   25    M=2
   26    GOTO32
   27    L=2
   28    M=0
   29    GOTO10
   30    DO31I=1,N
   31    X(I,2)=X(I,1)
   32    SUMX1=0
   33    SUMX2=0
   34    DO36I=1,N
   35    SUMX1=SUMX1+X(I,1)
   36    SUXM2=SUMX2+X(I,2)
         LAG=LAGL
   37    IF(LAG)76,38,38
   38    IK=N-LAG
         SUMLP=0
```

```
          PSUMX1=0
          PSUMX2=0
          DO41I=1,IK
          I2=I+LAG
39        SUMLP=SUMLP+X(I,1)*X(I2,2)
40        PSUXM1=PSUMX1+X(I,1)
41        PSUMX2=PSUMX2+X(I2,2)
53        A=N
57        B=N-LAG
58        AVELP=(A*SUMLP-SUMX2*PSUMX1-SUMX1*(PSUMX2-SUMX2*B/A))/A**2
59        PRINT100,LAG,AVELP
          IF(LAG)74,60,74
60        IF(M-1)13,63,74
63        SIGMA=SQRTF(AVELP)
64        AVEX1=SUMX1/A
65        SPRDL=-F*SIGMA
66        SPRDU=F*SIGMA
67        SPRDEC=D*SIGMA
          SPRD=SPRDL
68        ACSUML=0
          ACSUMG=0
69        DO71J=1,N
          IF(AVEX1+SPRD-X(J,1))70,71,71
70        ACSUMG=ACSUMG+1.0
          ACSUML=ACSUML-1.00
71        ACSUML=ACSUML+1.0
72        PRINT101,SPRD,ACSUMG,ACSUML,SIGMA,AVEX1
          IF(SPRD-SPRDU)73,74,13
73        SPRD=SPRD+SPRDEC
          GOTO68
74        IF(LAG-LAGU)75,13,13
75        LAG=LAG+LAGDEC
          GOTO37
76        IL=N+LAG
          SUMLP=0
          PSUMX1=0
          PSUMX2=0
          DO79I=1,IL
          I2=I-LAG
77        SUMLP=SUMLP+X(I2,1)*X(I,2)
78        PSUMX1=PSUMX1+X(I2,1)
79        PSUMX2=PSUMX2+X(I,2)
          B=N+LAG
          A=N
          GOTO58
          END
```

2. Power spectral function

```
          DIMENSION Y(100,1)
          COMMONY
```

```
  1     FORMAT(6I4,3F7.2)
  2     FORMAT(2I4,F12,5)
100     FORMAT(1H,6I6,3F9.2)
101     FORMAT(2I5,F12.5)
102     FORMAT(3E20.8)
103     FORMAT(4E20.8)
  5     READ1,M,N,L,LAGL,LAGU,LAGDEC,FRQL,FRQU,FRQDEC
        PRINT100,M,N,L,LAGL,LAGU,LAGDEC,FRQL,FRQU,FRQDEC
  7     I=1
  8     READ2,ID1,ID2,Y(I,L)
        PRINT101,ID1,ID2,Y(I,L)
 10     IF(ID1-2)11,12,11
 11     STOP89
 12     IF(ID2-1)11,13,11
 13     DO17I=2,N
 14     READ2,ID11,ID22,Y(I,L)
        PRINT101,ID11,ID22,Y(I,L)
 15     IF(ID11-ID1)11,16,11
 16     IF(ID22-ID2-1)11,17,11
 17     ID2=ID22
 18     IF(M-1)11,27,41
 27     FRQ=FRQL
 28     SUMCOS=0
 29     LAG=LAGL
 30     DO33I=1,N
 31     A=LAG
 32     SUMCOS=SUMCOS+Y(I,L)*COSF(A*FRQ*0.05235988)
 33     LAG=LAG+LAGDEC
        TRANS=SQRTF(SUMCOS)
 36     PRINT102,FRQ,SUMCOS,TRANS
 37     IF(FRQ-FRQU)38,11,11
 38     FRQ=FRQ+FRQDEC
 39     GOTO28
 41     IF(M-2)11,42,11
 42     FRQ=FRQL
 43     SUMCOS=0
 44     SUMSIN=0
 45     LAG=LAGL
 46     DO50I=1,N
 47     A=LAG
 48     SUMCOS=SUMCOS+Y(I,L)*COSF(A*FRQ*0.05235988)
 49     SUMSIN=SUMSIN+Y(I,L)*SINF(A*FRQ*0.05235988)
 50     LAG=LAG+LAGDEC
        CMAG=SQRTF(SUMCOS**2+SUMSIN**2)
 53     PRINT103,FRQ,SUMCOS,SUMSIN,CMAG
 54     IF(FRQ-FRQU)55,11,11
 55     FRQ=FRQ+FRQDEC
 56     GOTO43
        END
```

3. Fortran abbreviations

The abbreviations used in the correlation function Fortran statements are as follows.

M=1	indicates an autocorrelation calculation.
M=2	indicates a crosscorrelation calculation.
L=1	for both calculations.
N=	number of observations.
LAGL=	smallest value of lag, in units of 1/120 second, to be used.
LAGU=	largest value of lag to be used.
LAGDEC=	the amount the lag is to be incremented for each loop.
F=	multiple of the standard deviation to be used in the probability density analysis.
D=	multiple of the standard deviation. The amount the amplitude interval is incremented for the probability density analysis is determined by the value of D.

The abbreviations used in the power spectral function Fortran statements are as follows.

M=1	indicates a power spectral calculation.
M=2	indicates a cross power spectral calculation.
L=2	for both calculations.
N=	number of observations.
FRQL=	smallest value of the frequency expressed in cycles per second to be used.
FRQU=	largest value of the frequency to be used.
FRQDEC=	the amount the frequency is to be incremented for each loop.

XIII. APPENDIX C

A. Other Measuring Techniques

The purpose of this section is to discuss other experimental methods of measuring power spectral density and correlation functions.

The auto and crosscorrelation functions can be determined directly by several different techniques. One might use a multi-channel mangetic tape recorder and record the ion chamber signals. The play back mechanism would be provided with a time delay mechanism so that both $x(t)$ and $x(t+\xi)$ could be obtained simultaneously. The signal and delayed signal would then be multiplied and integrated on an analog computer. The time average value of the product of the two signals is proportional to the correlation function. Because of the low frequency response required it is desirable to use an F.M. system. An alternate technique might be to record the signals on film and pass the film between a photoelectric cell and light source. A time delay mechanism could be provided and the signal and delayed signal analyzed in the same manner as for magnetic tape.

Both of the previous methods have the disadvantage that accuracy is limited by the accuracy of the analog computer equipment used. In order to overcome this difficulty a direct digital data acquisition system can be used. With this system the ion chamber signals would be converted to digital information and then processed directly on a digital computer. There would be no need for the intermediate use of an analog computer.

The power spectral and cross power spectral density functions can be determined directly by analog computer techniques. The disadvantage here is again the accuracy that can be obtained. The technique is based

upon the relationship

$$\overline{x^2(t)} \alpha \int_{-\infty}^{\infty} \Lambda(\omega)\, d\omega \ , \tag{113}$$

where $\Lambda(\omega)$ is the power spectral density and $x(t)$ is the signal to be analyzed. Equation 113 states that the mean square value of $x(t)$ is proportional to the total power present in the signal. Most physical measurements can be converted to a voltage. This voltage is applied to the input of the circuit of Figure 16. The random signal is passed through a tuneable bandpass filter with the pass band centered at ω^1 and with pass band width $\Delta\omega^1$. The output of the filter contains mostly frequency components of $x(t)$ in the band width $\Delta\omega^1$ since the components outside the pass band are greatly attenuated. The signal is then passed through a squaring device and integrated. The output of the integrating amplifier is proportional to the mean square value of $x(t)$. In the actual measurements one is restricted to finite averaging times and only positive frequencies are present of course.

An expression for the power spectral density can be derived formally as follows. The mean square value of $x(t)$ with frequency components in $\Delta\omega^1$ can be written as

$$\overline{x^2_{\omega^1}} = \frac{1}{T} \int_0^T x^2(t)_{\omega^1}\, dt, \tag{114}$$

and Equation 113 for this case becomes

$$\overline{x^2}_{\omega^1} \alpha \int_{\omega_1}^{\omega_2} \Lambda(\omega)\, d\omega \tag{115}$$

where $\omega_2 - \omega_1$ is the band width of the filter. If $\Lambda(\omega)$ is approximately constant over the bandwidth, Equation 115 can be written as

$$\overline{x^2}_{\omega^1} \alpha \Lambda(\omega^1)\Delta\omega^1 . \tag{116}$$

By combining Equations 115 and 116 the following relationship for $\Lambda(\omega^1)$ is obtained;

$$\Lambda(\omega^1) \alpha \frac{1}{\Delta\omega^1 T} \int_0^T x^2(t)_{\omega^1} dt . \tag{117}$$

By changing the midband frequency of the band pass filter the power spectral density function can be determined as a function of frequency. In words, $\Lambda(\omega)$ is the average power contained in a frequency band width $\Delta\omega$ divided by the band width.

The measurement of cross power spectral density functions is more complex than the power spectral measurements since both real and imaginary parts must be determined. The circuits required to do this are shown in Figure 17. The two signals x(t) and y(t) are passed through identical band pass filters set at the midband frequency ω^1. One signal is shifted 90 degrees and multiplied times the unshifted signal to generate the imaginary part. The real part is obtained from the product of the two unshifted signals.

Expressions for the two parts of the cross power spectral function can be derived as follows. An approximation to the Fourier transform pair of correlation function and power spectral density can be written as

$$\frac{1}{T} \int_0^T x(t) \Big]_{\omega^1} y(t+\xi) \Big]_{\omega^1} dt = \int_{\omega_1}^{\omega_2} \Lambda_{xy}(\omega) e^{j\omega\xi} d\omega , \tag{118}$$

where a finite integrating time is used in the definition of the correlation function and a finite band width is used for the inverse Fourier transform. x(t) and $y(t+\xi)$ are assumed to contain only frequencies in $\omega_2 - \omega_1$.

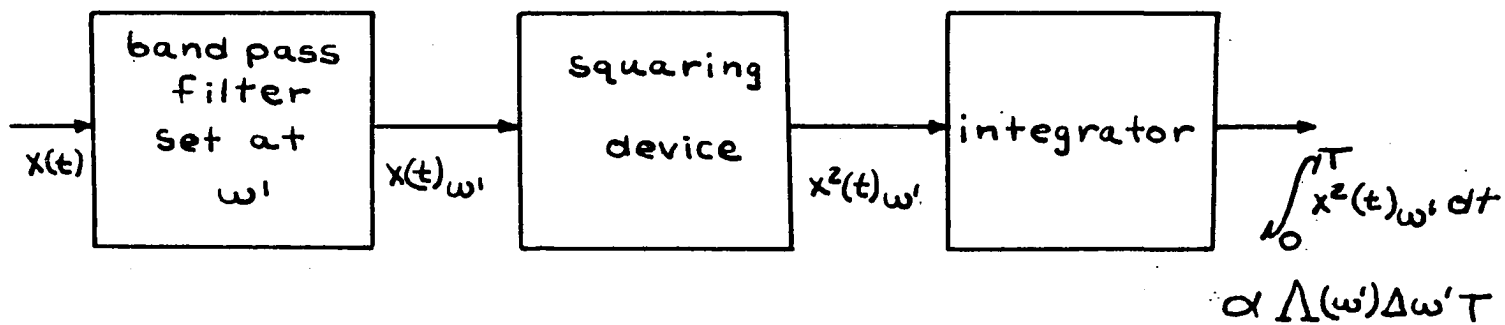

Figure 16. Components required for power spectral density measurements

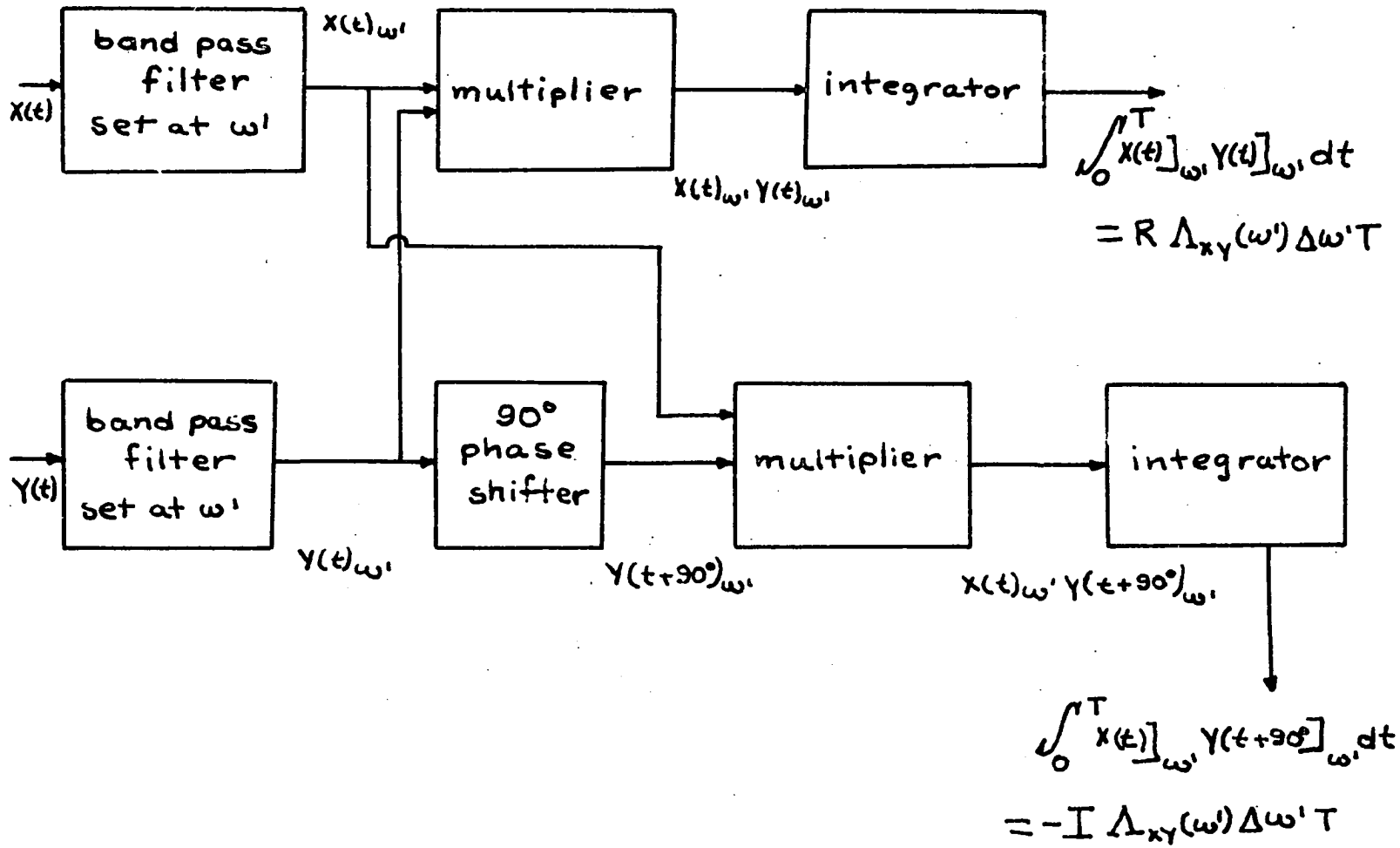

Figure 17. Components required for cross power spectral density measurements

If the power spectral density is constant in the band width $\omega_2 - \omega_1$, Equation 118 can be written as,

$$\frac{1}{T}\int_0^T x(t)\Big]_{\omega^1} y(t+\xi)\Big]_{\omega^1} dt = \Lambda_{xy}(\omega^1)e^{j\omega^1\xi}\Delta\omega^1 . \qquad (119)$$

From Euler's relation;

$$e^{j\omega^1\xi} = \cos\omega^1\xi + j\sin\omega^1\xi , \qquad (120)$$

so Equation 119 reduces to

$$\frac{1}{T}\int_0^T x(t)\Big]_{\omega^1} y(t+\xi)\Big]_{\omega^1} dt$$

$$= [R\Lambda_{xy}(\omega^1)\cos\omega^1\xi - I\Lambda_{xy}(\omega^1)\sin\omega^1\xi + j(I\Lambda_{xy}(\omega^1)\cos\omega^1\xi + R\Lambda_{xy}(\omega^1)\sin\omega^1\xi)]\Delta\omega^1 , \qquad (121)$$

where $R\Lambda_{xy}(\omega^1)$ represents the real part of $\Lambda_{xy}(\omega^1)$ and $I\Lambda_{xy}(\omega^1)$ the imaginary. If ξ is zero, Equation 121 becomes

$$\frac{1}{T}\int_0^T x(t)\Big]_{\omega^1} y(t)\Big]_{\omega^1} dt = [R\Lambda_{xy}(\omega^1) + jI\Lambda_{xy}(\omega^1)]\Delta\omega^1 . \qquad (122)$$

The integral is a real quantity so that when real parts are equated

$$R\Lambda_{xy}(\omega^1) = \frac{1}{\Delta\omega^1 T}\int_0^T x(t)\Big]_{\omega^1} y(t)\Big]_{\omega^1} dt. \qquad (123)$$

If ξ is set equal to $\pi/2\omega^1$ in Equation 121 and the relationship

$$y(t + \frac{\pi}{2\omega^1})\Big]_{\omega^1} = y(t + 90^\circ)\Big]_{\omega^1} \qquad (124)$$

is used, it follows that

$$\frac{1}{T}\int_0^T x(t)\Big]_{\omega^1} y(t + 90^\circ)\Big]_{\omega^1} dt = \Big[-I\Lambda_{xy}(\omega^1) + jR\Lambda_{xy}(\omega^1)\Big]\Delta\omega^1 . \qquad (125)$$

Equating real part again yields

$$I\Lambda_{xy}(\omega^1) = -\frac{1}{\Delta\omega^1 T}\int_0^T x(t)\Big]_{\omega^1} \quad y(t+90^\circ)\Big]_{\omega^1} \, dt. \tag{126}$$

Equation 126 is approximately valid since it can be assumed that the major frequency components in x(t) and y(t) are around ω^1.

Thus by the use of Equation 123 and 126 the two parts of the cross power spectral density function can be determined. This technique was used for power spectral measurements in the UFTR at the University of Florida.[1]

---

[1]Uhrig, Robert E. Gainesville, Florida. Cross power calculation. Pivate communication. 1963.